Dorsal tegmental dopamine neurons gate associative learning of fear

Florian Grössl[1], **Thomas Munsch**[#2], **Susanne Meis**[#2], **Johannes Griessner**[1,3], **Joanna Kaczanowska**[1], **Pinelopi Pliota**[1], **Dominic Kargl**[1], **Sylvia Badurek**[4], **Klaus Kraitsy**[4], **Arash Rassoulpour**[5], **Johannes Zuber**[1], **Volkmar Lessmann**[2], and **Wulf Haubensak**[1,*]

[1]Research Institute of Molecular Pathology (IMP), Vienna Biocenter (VBC), Campus-Vienna-Biocenter 1, 1030 Vienna, Austria

[2]Institute of Physiology (Medical Faculty), and Center for Behavioral Brain Sciences (CBBS), Otto-von-Guericke University, Leipziger Str. 44, 39120 Magdeburg, Germany

[3]Medical University of Vienna, Spitalgasse 23, 1090 Vienna, Austria

[4]Preclinical Phenotyping Facility, Vienna Biocenter Core Facilities (VBCF), Vienna Biocenter (VBC), Dr. Bohr Gasse 3, 1030 Vienna, Austria

[5]Brains On-Line, Charles River Laboratories), San Francisco, USA

[#] These authors contributed equally to this work.

Abstract

Functional neuroanatomy of Pavlovian fear has identified neuronal circuits and synapses associating conditioned stimuli with aversive events. Hebbian plasticity within these networks requires additional reinforcement to store particularly salient experiences into long-term memory. Here, we have identified a circuit reciprocally connecting the ventral periaqueductal grey (vPAG)/dorsal raphe (DR) region and the central amygdala (CE) that gates fear learning. We found that vPAG/DR dopaminergic (vPdRD) neurons encode a positive prediction error in response to unpredicted shocks, and may reshape intra-amygdala connectivity via a dopamine-dependent form of long-term potentiation (LTP). Negative feedback from the CE to vPdRD neurons might limit reinforcement to events that have not been predicted. These findings add a new module to the midbrain DA circuit architecture underlying associative reinforcement learning and identify vPdRD neurons as critical component of Pavlovian fear conditioning. We propose that dysregulation of vPdRD neuronal activity may contribute to fear-related psychiatric disorders.

[*]To whom correspondence should be addressed.

Introduction

The brain uses predictors of important events to optimize future behavioral responses. Pavlovian learning pairs a stimulus with an emotionally salient experience to form emotional memories that can be stored for life[1]. Deconstructing the neuronal basis of storage and recall of such associative memories and the underlying learning models promises insight into fundamental and biomedically relevant brain functions.

The primary neuronal representation of associations between conditioned stimulus (CS) and unconditioned stimulus (US)(CS-US pairing) is stored as synaptic memory traces in neuronal circuitry[2]. While Hebbian plasticity (coinciding pre- and postsynaptic activity) accounts for the primary CS-US pairing, additional processes are required to link associative plasticity to particularly salient events and to the progress in learning itself. Reinforcement signals coupled to prediction errors (PE; a central element in learning models representing the discrepancy between the value of actual and predicted events) can serve that purpose. However, neuronal circuit motifs encoding all necessary components for associative learning, i.e., CS-US integration, PE-coupled reinforcement signals and synaptic memory trace, remain largely uncharted.

In the mammalian brain, Pavlovian fear-related neuronal plasticity in the amygdala is the canonical model for storage of associative memory traces[1]. Within the amygdala, the central amygdala (CE) operates as central hub that re-shapes neural responses[3,4] and synaptic connectivity during learning[5]. In this regard, neurons in the lateral part of the CE (CEl) can be functionally divided into several classes of distinguishable inhibitory neurons, which receive excitatory input from the basolateral amygdala (BLA). Fear learning leads to postsynaptically expressed LTP of the input onto $SST^+/PKC\delta^-$ neurons[5], whose activity correlates with aversive fear states in various fear-related behavioral assays[3,4,6].

Dopamine (DA) is the canonical link between PE and synaptic reinforcement signals modulating Hebbian plasticity rules of CS-US associations[7]. Foremost identified as key mediator of reward learning[8,9], DA neurons may also drive aversive learning[10–12], suggesting a general role in both negative and positive reinforcement learning. DA modulates neural activity in the CEl via DA1-like and DA2-like receptors (D1R, D2R)[13,14], making it a promising candidate for experience dependent rewiring of amygdala connectivity.

Although evidence for aversive signaling in VTA DA neurons (the midbrain DA neurons for appetitive reinforcement) has been reported[15], the majority of studies observed inhibition[16–18] or no response at all[8,9,19] in response to aversive signals. This raised the obvious question whether other DAergic neurons outside the VTA reward system might provide DA driven aversive teaching signals for CE fear learning. Interestingly, a relatively neglected group of DA neurons in the ventral PAG/dorsal Raphe (vPdRD neurons)[20–22] represent a particularly promising candidate: although optogenetic stimulation of vPdRD neurons modulates social behavior[21], it does not reinforce operant responses[23], functionally separating these vPdRD from VTA DA neurons[24]. Moreover, the vPAG itself can encode

aversive teaching signals25,26 as it integrates afferent, aversive somatosensory and nociceptive information while being an output structure for various fear-conditioned responses.

Taken together, the CE and the midbrain DA system emerged as promising entry points in our search for circuit motifs integrating Hebbian memory traces and reinforcement signals in associative learning. Synaptic tracing and circuit mapping revealed vPdRD neurons as major source of DAergic projections to the CE. Suppression of vPdRD neuron activity diminished fear learning, accompanied by reduction of experience dependent potentiation of the BLA-CE SST[+] synapses. Notably, vPdRD neuronal activity shifted from US to CS as learning progressed, linking experience dependent CE rewiring to the animals' PE. We tested this by optogenetically modulating PE signals in vPdRD neurons during associative learning. Reducing PE-related neuronal activity decreased Pavlovian fear learning. Conversely, increasing PE-related neuronal activity interfered with associative blocking. Taken together, these results delineate a learning circuit of reciprocally connected vPdRD and CE neurons, and demonstrate how neural systems integrate reinforcement signals with CS-US associations to write experiences into long-term memory. We assign a defined function to vPdRD neurons and identify them as a critical element for associative learning.

Results

The vPAG/DR provides a major DAergic input to the CE

Tyrosine hydroxylase (TH) immunohistochemistry (IHC) in mice highlight the CE as one of the most densely innervated DA targets in the temporal lobe (Fig. 1a). Although projections to CE from canonical DA-ergic midbrain sources (i.e. substantia nigra (SN) and ventral tegmental area (VTA); compare Fig. 1b), have been reported27–29, combined CE Cholera toxin B (CTB; retrograde synaptic marker) injections (Fig. 1c) and TH IHC (Fig. 1d), mapped the majority of DA-ergic afferents to a group of vPdRD neurons (Fig. 1e) of largely unknown function (but see21,22). Moreover, a large fraction of these neurons throughout the rostral – caudal extension of vPAG/DR (Fig. 1f), projects to the CE, and particularly to CEl, with surprising specificity (Supplementary Fig. 1), whereas DAergic projections from SN and VTA to the amygdala in general, appear to be rather sparse (Supplementary Fig. 2). Collectively, these data establish a potential link between vPdRD neurons, Pavlovian fear conditioning and DA modulation of CE circuitry.

We therefore investigated the synaptic connectivity of vPdRD neuron projections to SST[+] and PKCδ^{+} cells, two major neuronal types in the CEl, in acute brain slices. We injected PKCδ::Cre/TH::Cre double transgenic mice with AAV::DIO-GFP into the CEl and AAV::DIO-ChR2-YFP into the vPAG/DR (Fig. 1g-i). Targeted electrophysiological recordings of postsynaptic CEl GFP[-] and GFP^{+} cells, considered identical with SST[+]/PKCδ[-] and PKCδ [+]/SST[-] neurons5 (Supplementary Fig. 3a), respectively, revealed direct excitatory post-synaptic currents in response to optogenetic presynaptic stimulation of CEl vPdRD neuron terminals (Fig. 1j), blocked by bath-application of CNQX and APV-5. Together with recent reports28,39, these data suggest that vPdRD neurons innervate, potentially co-release glutamate and DA21, into the CEl in vivo. While the fraction of responding cells (Fig. 1k) and the signal amplitude in responding neurons (Fig. 1l) was

similar between cell types, the overall location of responding neurons was spatially biased to the medial part of the CEl at the CEl/m transition boundary (Fig. 1m), congruent with the vPdRD neuron innervation pattern (Fig. 1a and 1i).

The vPdRD neuron - CE axis features characteristics of a learning circuit

We reasoned that this specific innervation from the vPAG/DR, a multimodal brain region involved in pain processing, might directly reinforce fear learning in the CE circuitry through Glu/DA co-release in response to aversive experiences. Indeed, fiber-endomicroscopic Ca^{2+} imaging in freely moving animals, injected with AAV-expressing GCaMP6m in the vPAG/DR (Fig. 2a, Supplementary Fig. 4a), showed strong bulk Ca^{2+} responses to the Pavlovian shock US (Fig. 2b) in this region, with neuronal subsets directly responding to the US (Fig. 2c).

These responses were accompanied by a shock-US specific rise in intra-amygdalar DA levels as observed through targeted microdialysis in freely moving animals during Pavlovian fear conditioning (Fig. 2d, Supplementary Fig. 5a). Note that for better feasibility the microdialysis was performed in rats, assuming a (gross) fear neuroanatomy similar to mice. These experiments must be interpreted with caution with respect to the stereo specificity of sampling site (CEl vs. BLA) and source (VTA vs. vPdRD neurons). First, the method samples amygdala DA across CEl and BLA. However, given the steep gradients in amygdala DA innervation (Fig. 1a, Supplementary Fig. 2), we believe that the majority of the sampled DA originates from CEl. Second, these experiments will also sample CE DA from VTA. However, most of CE (and amygdala) DAergic innervation stems from vPdRD neurons and not from VTA (Fig. 1e, Supplementary Fig. 2). Jointly with the fact that vPdRD neurons are active during shock (Fig. 2c) and have been shown to increase CE DA21 it seems likely that a large part of shock induced DA observed (Fig. 2d) originates from vPdRD neurons and CE. Notably, the increase in amygdalar DA was absent during re-exposure to the shock-context (CS) 24 h later (Fig. 2d), consistent with a role for CE DA in aversive reinforcement learning.

To determine whether DA re-shapes CE synaptic connectivity, we examined DA-ergic modulation of BLA to CE synapses, which potentiate during Pavlovian fear conditioning5. We first probed glutamaterigc synapses onto CEl neurons for activity-dependent plasticity in response to high-frequency stimulation (HFS) of BLA inputs using acute slice electrophysiology (Fig. 2e). HFS induced synaptic plasticity of evoked local field potentials (LFPs) in the CEl increased in the presence of DA30. To assess the cell-type specificity of this potentiation, we performed single cell whole cell patch-clamp recordings and filled recorded neurons with biocytin for post-hoc classification of neuronal subtypes (Supplementary Fig. 3a). Under basal conditions, the major (SST$^+$/PKCδ$^-$ and PKCδ$^+$/SST$^-$) CEl cell types failed to undergo LTP after HFS stimulation of BLA inputs (Supplementary Fig. 3b). However, application of DA specifically gated LTP of excitatory BLA inputs onto CEl SST$^+$/PKCδ$^-$ cells (Fig. 2f), but not PKCδ$^+$/SST$^-$ neurons. This effect was blocked by the D1R antagonist SCH 23390 (Fig. 2g). Population specific transcriptional profiling of FACS-sorted neurons from Cre-dependent td-Tomato reporter mouse lines crossed to either SST::Cre or PKCδ::Cre animals revealed higher expression of D1Rs in SST$^+$/PKCδ$^-$

neurons (Supplementary Fig. 6). These data suggest that cell-type specific DA dependent LTP (Fig. 2f) may be mediated by post-synaptic D1R signaling. The asymmetric distribution of D1Rs could specifically sensitize SST⁺/PKCδ⁻ neurons for fear-related associations and map aversive states asymmetrically on genetically and functionally pre-defined SST⁺/PKCδ⁻ neurons. These data might explain how fear conditioning could teach SST⁺/PKCδ⁻ neurons to respond to tone-CSs4,31, selectively strengthen their responses to BLA input5 and ultimately link them to aversive states31.

Taken together, DA, likely released from vPdRD neuron afferents, contributes to cell type specific potentiation of a BLA-to-CE fear synapse to gate associative learning of Pavlovian fear. Therefore, we examined if successful acquisition, storage and/or expression of fearful experiences of animals may require vPdRD neuronal activity.

vPdRD neurons control associative learning of fear

We injected Cre-dependent AAV into the vPAG/DR of TH::Cre animals for selective expression of Clozapine N-Oxide (CNO) activatable receptors exclusively activated by designer drugs (M4-DREADD, AAV::DIO-M4) in vPdRD neurons (*M4-cohort* in Supplementary Fig. 7a). These animals received intra-peritoneal CNO injections 30 min prior the conditioning phase. This treatment, expected to hyperpolarize and electrically silence vPdRD neurons, resulted in decreased freezing responses to the CS during training (Fig. 3a-b). Notably, this cohort showed significantly less freezing than controls during (drug-free) recall the next day. These results establish a critical role for vPdRD neurons in fear learning. Silencing vPdRD neurons with M4 did not lead to overt differences in the elevated plus maze or light/dark transition test (Supplementary Fig. 8a-b), indicating that these cells do not directly modulate anxiety states.

We next tested whether input from vPdRD neurons is required for experience dependent rewiring of CE circuitry. To this end, we ablated vPdRD neurons with stereotactic injections of the neurotoxin 6-hydroxydopamine (6-OHDA) into the vPAG/DR (Supplementary Fig. 7b), and post hoc determined synaptic weights of BLA-CEl connectivity (Fig. 3c; compare next paragraph), after fear conditioning (FC). As expected, ablating vPdRD neurons impacted fear learning and recall, similarly to the effects observed in our DREADD cohort earlier (Fig. 3d). Note that 6-OHDA neurotoxicity towards vPdRD neurons, which lack dopamine-β-hydroxylase32, provides direct evidence that these cells are indeed DAergic.

Next, we isolated acute slices from these lesioned animals and recorded excitatory postsynaptic currents (EPSCs) in neighboring SST⁺ and PKC-δ⁺neuronal pairs after electrical stimulation of BLA inputs. Interestingly, EPSC amplitudes were increased selectively in SST⁺ neurons after fear conditioning, resulting in a shift of synaptic weights from BLA-to-PKC-δ⁺/SST⁻ towards BLA-to-SST⁺/PKC-δ⁻synaptic connectivity (Fig. 3e-f, FC vs. home cage (HC) cohorts). These results are in line with previous studies5 and indicates that fear conditioning rewires BLA-CE circuitry in a cell type specific manner.

In 6-OHDA lesioned animals, in which ablation of vPdRD neurons decreased fear memory formation (Fig. 3c-d), the fear conditioning induced shift of synaptic weights was markedly reduced and not significantly different from the HC cohort (Fig. 3f). Furthermore, the

excitatory drive, determined as frequency and amplitude of spontaneous EPSCs recorded in SST$^+$ and PKC-δ$^+$ neurons, resembled the HC state in 6-OHDA lesioned animals (Supplementary Fig. 9). Thus, selectively ablating vPdRD neurons and thereby eliminating their inputs to the CE resulted in fear memory deficits, which were accompanied by failure to rewire BLA-CE connectivity.

Following the observation of D1R dependent cell type specific gating of LTP at BLA-CEl synapses, we next probed if experience-dependent synaptic plasticity in the CE and fear memory were dependent on CEl D1R signaling. Indeed, RNAi-mediated knockdown of CE1 D1R through injection of AAV viruses expressing GFP-linked shRNAs before fear conditioning (Supplementary Fig. 10a-e) resulted in a similar shift in BLA-CE connectivity as observed in 6-OHDA lesioned animals (Fig. 3f) and fear memory deficits at recall (Supplementary Fig. 10f). Together, these results suggest that vPdRD neuronal activity and asymmetric D1R signalling in CE may underlie a fear memory trace in BLA-CE connectivity.

The comparably mild behavioral phenotype of the D1R knock down experiment (Supplementary Fig. 10) in comparison with the noticeable synaptic effects (Fig. 3e) may be attributed to the fact that slice electrophysiology records specifically from neurons infected with D1R knock down virus, whereas D1R knockdown efficiency in the CE might have been too low to strongly affect behavior, also in comparison to the DREADD silencing (Fig. 3b) and 6-OHDA lesions (Fig. 3d). To interfere with D1R signaling in the CEl more efficiently, we cannulated mouse cohorts bilaterally over the CEl for infusion of the D1R antagonist SCH23390 (Fig. 3g, Supplementary Fig. 5b). Similar to the circuit genetic perturbation using M4-DREADDs (Fig. 3a, b) this manipulation did not alter anxiety (Supplementary Fig. 8c-d). In contrast to the M4-DREADD-silenced cohort (Fig. 3b), pre-training SCH23390 infusion did not result in significantly different freezing responses during training. However, drug-free fear memory recall was strongly decreased (Fig. 3h), similarly to our observations in the M4-DREADD cohort (Fig. 3b). Thus, simultaneous blocking of Glu- and D1R-signaling perturbs short- and long-term fear memory, whereas blocking D1Rs selectively prevents long-term fear memory formation and leaves short-term memory intact. Hypothetically, these data may dissociate Glu- and DA-components of vPdRD signaling: Glu could control short-term memory, whereas DA co-release may primarily consolidate long-term associative memory at BLA-to-CEl SST$^+$/PKCδ$^-$ synapses.

Collectively, these data suggest that vPdRD neurons sense aversive USs to gate memory formation in the amygdala circuitry.

vPdRD neurons and the CE form a learning circuit

As components of DAergic reinforcement systems, vPdRD neurons should be most active when important events have not been predicted (large positive PE) and decrease activity with the progress in learning – a notion supported by the fact that the PAG has the capacity to signal aversive PEs in both, rats[25] and humans[33]. The most intuitive implementation of such negative feedback from learning would be direct inhibition of DA neurons by CEl SST$^+$/PKCδ$^-$ cells – or CEm (the major CE output), the elements that "learn" with conditioning. Indeed, PAG targeted CTB injections revealed retrogradely labelled neurons in the CEl,

originating predominantly from SST$^+$/PKCδ$^-$ neurons (Supplementary Fig. 11). This was supported by bilateral AAV::DIO-ChR2 injections in the CE of SST::CRE and PKCδ::CRE mice, showing rather selective vPAG/DR innervation from SST$^+$/PKCδ$^-$ neurons (Supplementary Fig. 11). Together with the strong retrograde labeling of the CEm (Supplementary Fig. 11), this indicates that SST$^+$/PKCδ$^-$ neurons, but not PKCδ$^+$/SST$^-$ neurons, and the CEm are the major CE sources for vPdRD neuron innervation.

To elucidate the inter-connectivity between CE and vPdRD neurons in more depth, we co-injected ChR2-YFP and CTB 555 in the CE for optogenetic manipulation of CE arising fibers connecting to vPdRD neurons (retrogradely labelled by CTB) that project back to the CEl (Fig. 4a). The DA-ergic nature of biocytin labelled recorded neurons was confirmed post hoc by TH IHC (Fig. 4b). Optogenetic stimulation of CE inputs evoked inhibitory PSCs in CEl projecting DA neurons in the PAG, sensitive to application of the GABA$_A$ receptor antagonist bicuculline (50 μM) (Fig. 4c). Thus, CEl SST$^+$/PKCδ$^-$ neurons and CEm may inhibit further reinforcement from vPdRD neurons, in particular after BLA-CE circuitry has learned to respond to, and predict, the fear US[4,31].

In search for the proposed modulation of vPdRD neuron activity during learning progress, we compared deep brain Ca^{2+} signals of vPdRD neurons expressing GCaMP6f (Fig. 4d-h, Supplementary Fig. 4b) during a series of two-reinforced (Fig. 4e-i; Cond. 1, Cond 2) and one non-reinforced (Fig. 4e-i; Recall) fear conditioning sessions. Freezing levels of animals confirmed that mice developed robust fear memories during CS-US association trials (Fig. 4e).

Bulk Ca^{2+} population signals from vPdRD neurons showed a strong increase in Ca^{2+} signals during CS-US pairings in the first conditioning (Supplementary Data 1; Supplementary Fig. 12e-f; Fig. 4f-g). As learning progressed to the second conditioning, the population Ca^{2+} signal of vPdRD neurons started to register the previously reinforced CS, whereas the population Ca^{2+} signal to the US, which could be predicted by the animal at this time point, decreased. During non-reinforced recall 24h later, after consolidation of fear memories, vPdRD neurons showed strong increase in Ca^{2+} signals to the CS, when compared to the conditioning sessions.

A similar picture emerged at the level of single units (Supplementary Videos 1-3; Supplementary Data 1; Supplementary Fig. 12f; Fig. 4h-i). Analysis of single unit Ca^{2+}signals (Fig. 4i) revealed a shift of the dominant response clusters from US- to CS-driven activity over the course of the paradigm. To investigate if this trend reflected discrete, stimulus driven neuronal firing (mirroring actual action potentials), we transformed the Ca^{2+} signals into neuronal activity events, defined as rise in Ca^{2+} signals above 3 median S.D. We then filtered for those units (referred to as responders) whose firing to either CS and/or US exceeded >95% CI of the expected mean activity (Supplementary Fig. 12f). Indeed, the population activity of these responders followed a similar pattern (Fig. 4j, *top*), with the fraction of responder types shifting from US to CS throughout the paradigm (Fig. 4j, *bottom*). Notably, these results are also contained within the vPAG/DR neuronal population as a whole (Supplementary Fig. 12a-d). Thus, vPdRD neurons appear to encode a positive PE in aversive reinforcement learning.

Stimulus associated activity of vPdRD neurons gates learning

If vPdRD neurons encode PE linked reinforcement signals, their activity during associations should critically modulate learning.

Thus, we examined whether optogenetic inhibition of vPdRD neurons during the four 20s CS-US pairings, a period that corresponds to the highest neuronal activity during fear conditioning (Fig. 4i), would be sufficient to recapitulate the behavioral consequences of M4-DREADD silencing (Fig. 3a-b). Selective optogenetic inhibition of Arch expressing vPdRD neurons (Fig. 5a, Supplementary Fig. 4), suppressing PE linked reinforcement signals during associative periods, resulted in less freezing behavior to CS during conditioning and impaired fear responses when tested the next day (Fig. 5b, Recall). This establishes a critical role for vPdRD neurons at the time of CS-US pairings, and for the conversion of these pairings into short- and long-term fear memory. Similarly to M4-DREADD inhibition, Arch-mediated silencing of vPdRD neurons did not influence nociception (Supplementary Fig. 8e-h), functionally dissociating these neurons from a general role of vPAG/DR in gating pain.

Hypothetically, activation of vPdRD neurons could be enough to induce plasticity in the CE in the absence of an instructive US (foot shock). To investigate this possibility, we performed Ch2R-driven optogenetic activation of vPdRD neurons during CS-pairings (Fig. 5a, lower panel, Supplementary Fig. 7d). This optogenetic activation was not sufficient to instruct aversive memories in the absence of real shock-USs (Supplementary Fig. 13). Interestingly, we observed that optogenetic vPdRD neuron activation evoked slow continuous movement (Fig. 5c, Supplementary Video 4). A similar observation has been made recently upon activation of a different neuronal population in the ventral vPAG/DR34.

Overall, these results are in line with a role of vPdRD neurons in primarily mediating PE coupled reinforcement learning without encoding an intrinsic valence per se.

As activation of vPdRD neurons could not replace an instructive US during aversive fear learning by itself, we asked whether it may rather gate fear memory and associative learning in response to those contingencies that are novel and informative. We therefore examined whether vPdRD neuronal activity interferes with associative blocking of compound conditioning, a conditioning variant sensitive to aberrant reinforcement learning25,35(Fig. 5d). Under normal conditions, linking a novel CS (CS B) to a US is blocked when the novel CS is co-presented with a CS (CS A) that is already associated with, and thus predicts, the subsequent US. This effect is also evident in our experiment, as controls froze significantly more to CS A than CS B, indicating successful blocking of the association between CS B and the US (Fig. 5d, *right*). In contrast, optogenetic activation of vPdRD neurons during compound CS-US presentations had two effects. It significantly increased the previously observed slow motion attend-like behavior (Fig. 5c) at the expense of freezing in that session (Fig. 5d, *middle*) and inverted the CS-response pattern during recall (Fig. 5e). Thus, artificially increasing PE and reinforcement learning during associative periods, results in establishing memories that are normally suppressed.

Taken together these experiments show that manipulation of stimulus-bound vPdRD neuronal activity – effectively simulating a larger or a smaller than actual PE at time of association - bidirectionally modulates fear learning. Thus, PE signals in vPdRD neurons, and DA reinforcement signals originating from vPdRD neurons positively gate associative learning.

Discussion

Learning from aversive experiences is one of the most basic and biomedically important brain functions. Here, we describe a circuit motif, reciprocally interconnecting vPdRD neurons with CE circuitry (Supplementary Fig. 14). It couples a positive aversive PE signal to DAergic reinforcement of an experience dependent memory trace at an amygdala fear synapse.

Amygdala nuclei are the canonical substrate for fear memory formation. However, the reinforcing mechanisms that rewire amygdala circuitry during learning are much less understood. Notwithstanding the known interaction between VTA DA and the amygdala, a longstanding missing element of fear learning was a dedicated DA system that allows aversive PE coupled reinforcement learning to modulate amygdala synaptic memory traces. In identifying vPdRD neurons as a major DA input to CE circuitry, we provide a circuit context that links vPAG/DR, which integrates nociceptive US-related information[36] and encodes PE information[26,37,38], to DA driven rewiring of BLA-CE connectivity.

In line with US responses of the vPAG region during acquisition of fear learning[26], we find that the response of vPdRD neurons shift from US to CS as learning progresses with conditioning. This re-orientation towards the predictive value of emotionally relevant information is in line with vPdRD neurons encoding PE coupled teaching signals. While PE coupled reinforcement signals are integral parts of several Pavlovian fear learning models, their neuronal implementation has not been fully resolved at the circuit level[25]. We propose that vPdRD neuronal activity and DA signals mirror features of the PE and of PE linked reinforcement signals of classical Rescorla-Wagner[39] and Pearce-Hall[40] models, positively encoding unpredicted aversive stimuli (Fig. 4i, Conditioning 1, Conditioning 2). As omissions of the shock-US in the non-reinforced session (Fig. 4i, Recall) were not positively signaled, most of vPdRD neurons implement a Rescorla-Wagner type PE. That said, some sets of cells in the vPdRD responded with delayed onset to the CS (Fig. 4i, Recall, middle cluster), which might assign a positive signal and Pearce-Hall type PE to US omissions. Thus, different vPdRD cells might encode segregated features of learning models as has been suggested for VTA[10]. This should inspire experiments dedicated at resolving the fine structure of PE signals in the vPdRD neurons and dissociate them from PE signals in VTA. A scenario in which VTA DA neuron activity signals positive reward prediction errors[10] whereas vPdRD cells signals positive fear prediction errors might be attractive, but is likely too simplistic.

Of note, DA release of vPdRD projections has been shown recently[21]. CE targeted retrograde tracing (Fig. 1c-f) identified vPdRD neurons as major DA neuronal input source whereas amygdalar projections from other dopaminergic areas beside vPdRD neurons

appear to be rather sparse (Supplementary Fig. 2). Although contributions from these areas cannot be ruled out, these observations point to vPdRD neurons as a major origin of DA ergic modulation in CE and perhaps the whole amygdala. Accordingly, we hypothesize that vPdRD neurons emit a DAergic teaching signal that adapts to the predictive value of a given CS. The CE, in turn, transforms this signal into fear memory. DA modulates synaptic plasticity of SST^{+} neurons in the CEl via D1R dependent LTP. This D1R mediated synaptic plasticity might contribute to the underlying mechanism of the fear experience dependent reshaping of BLA synapses onto CEl SST^{+} neurons (Fig. 3e)[5]. The fact that 6-OHDA lesions of vPdRD neurons can partially revert this effect, links aversive teaching signals from vPdRD neurons to DA mediated synaptic plasticity in the CEl. Since D1R potentiates BLA to CE synapses [13,14] and learning[41,42] and given that in our hands blocking of CE D2R signaling showed less behavioral consequences in fear conditioning (data not shown), we focused on D1Rs in our circuit model. However, we would like to point out that also D2R effects might contribute. In fact, our sequencing results show D2R expression in both CEl cell types (data not shown). Thus, CE D2R signalling may synergize with D1R activation to induce experience- and vPdRD neuron-dependent rewiring of BLA-CE SST[+]/ PKCδ[+] connectivity. Importantly, such a mechanism integrates earlier work[43] into the circuit framework put forward by our study. The complexity of DA receptor signaling in the amygdala[43,44], demands further studies to dissociate the role of D1R vs. D2R dependent mechanisms.

It has recently been shown that CE feedback to the vlPAG controls fear learning, stimulus responsivity of vlPAG neurons and PE coding in the amygdala[38]. Our results extend the possible explanation for this observation as we find direct inhibitory synaptic connectivity of CE output from CEl SST[+]/PKCδ^{-} cells and CEm to vPdRD neurons (Fig.4). During fear learning, this negative feedback projection could regulate vPdRD neurons and henceforth adapt PE signaling according to the neuronal activity state in CEl and CEm (e.g., suppression of US responding by a preceding predictive CS after CS learning by SST[+]/ PKCδ^{-} CEl neurons).

We used a combination of fear conditioning and an associative blocking design[25] to assess whether manipulation of vPdRD neuronal activity modulates associative learning. Silencing vPdRD neuronal activity during CS-US pairings, thereby simulating a PE that is smaller than actual, resulted in decreased CS-US associations. Conversely, increasing activity during CS-US compound pairings in associative blocking, simulating a PE that is larger than actual, facilitated the association of the novel CS (CS B). Thus, modulation of vPdRD activity, presumably representing PE coupled reinforcement, gates learning. In contrast to VTA DA neurons, where direct activation can induce behavioral conditioning[45] or reinforcement, our results demonstrate that this is not the case for sole activation of vPdRD neurons. This dissociates this class of DA neurons from VTA neurons. Moreover, it indicates that, besides vPdRD neuron activity, additional signals are required to write experiences into synaptic long-term memory in CE circuitry. In the context of aversive experiences, these US pain related signal may come from other brainstem systems[46]. Hence, vPdRD neuron activity retains a primarily reinforcing nature but does not encode an intrinsic affective valence.

Regardless, activation of vPdRD neurons in a neutral context led to a mild behavioral switch, manifested as constant slow movement. This type of behavior has been described recently for the ventral PAG as 'slow motion' behavior34. Notably, it was able to override freezing behavior in our associative blocking assay (Fig. 5c), while increasing associative performance. Thus, vPdRD neurons may drive an own-standing distinct attentive-like behavioral state.

A notable aspect of our study being in line with recent findings21, is the observation that vPdRD neurons can co-release glutamate in the CEl. The co-release of DA together with either one of the fast ionotropic neurotransmitters like GABA and glutamate has been observed for VTA DA neurons previously47 but there is no satisfying theory about how it could affect behavior. Strikingly, blocking of DA in the CEl only affected fear testing (Fig. 3g-h), whereas optogenetic inhibition of vPdRD neurons, that most likely blocks the majority of DA and glutamate release in the CEl, affects short term fear memory during the conditioning phase as well (Fig. 5). One attractive hypothesis is, that glutamate co-release facilitates short term learning, which DA reinforces to long term synaptic memory, functionally dissociating these co-released neurotransmitters. Interestingly, glutamate activates PKCδ$^+$/SST$^-$ neurons (Fig. 1k) which could drive short term learning by increasing attention-like states via the basal forebrain48,49. The 'slow motion' behavior evoked with very short delays after vPdRD neuron activation, likely driven largely by fast glutamate signaling from vPdRD neurons (rather than by the more slowly acting DA), may reflect such attention-like states.

Taken together, we identified a circuit motif, interconnecting vPdRD neurons and amygdala, that integrates the main components of associative learning (CS/US information, PE and synaptic memory) to shape an amygdala fear response. DA release in the CEl acts as a retrograde reinforcement signal by setting synaptic learning rules7 to control Pavlovian memory traces. An inhibitory feedback-loop may inhibit reinforcement signals to prevent excessive associations. This delineates an intuitive model (Supplementary Fig. 14) on how the brain computes a learning problem. In the context of aversive learning, the vPdRD component integrates nociceptive US-related information and - via direct interaction with the CE - signals the PE to reinforce plasticity at a CEl fear synapse.

The dopaminergic identity of vPdRD neurons has previously been suggested21,22 and our 6-OHDA lesion results further proof this notion. Thus, our study assigns a defined neuronal circuitry and behavioral function to vPdRD neurons, a hitherto relatively uncharted class of DA neurons in the mammalian brain.

In turn, we identify vPdRD neurons as a central component for negative reinforcement learning. Importantly, the CE is a critical component of reward conditioning44, which might point towards a more general role of vPdRD-CE circuitry also in positive reinforcement learning. Together with the fact that DA-ergic neurons in general12 and the vPAG/DR region25 play a key role in learning processes, vPdRD neurons might emerge as central gatekeepers of associative reinforcement learning.

From a biomedical point of view, signatures of aversive PEs have recently been detected in the human PAG33. Thus, dysregulation of vPAG/DR DA-CE circuitry could lead to inadequate fear memories observed in PTSD, and, given the pain sensing properties of vPAG/DR, the comorbidity of PTSD and chronic pain50.

Accession codes

Neural population sequencing data (record GSE95154) are available at https://www.ncbi.nlm.nih.gov/geo/query/acc.cgi?token=oretwkoofbeppmp&acc=GSE95154.

Materials and Methods

Subjects

2-4 months old male mice were group housed (2-5 animals) in a colony on 14 h light/10 h dark cycle starting at 07:00 with food and water *ad libitum*. All animal procedures were performed in accordance with institutional guidelines and were approved by the respective Austrian (BGBl nr. 501/1988, idF BGBl I no. 162/2005) and European authorities (Directive 86/609/EEC of 24 November 1986, European Community) and covered by the license M58/002220/2011/9. C57BL/6J wild-type mice were in-house bred and provided after weaning from the Research Institute of Molecular Pathology (IMP) mouse facility. Prkcd::GluClα-Cre BAC transgenic mice (PKCδ::Cre)4, 7630403G23Rik$^{Tg(Th-cre)1Tmd}$ transgenice mice (TH::Cre, stock no008601, Jackson Laboratory), SOM-IRES-Cre transgenic mice (SST::Cre; stock no: 013044, Jackson Laboratory) and B6;129S6-$Gt(ROSA)26Sor^{tm9(CAG-tdTomato)Hze}$/J transgenic mice (Rosa::loxP-STOP-loxP-td-Tomato, stock no007909, Jackson Laboratory) were maintained heterozygous on a C57BL/6J background. Cohort sizes for neuroanatomical tracing approx. 30 2-4 months old male mice, slice electrophysiology approx. 50 1-3 months old male mice, microdialysis 4 adult male rats, GCaMP6m 2 2-3 months old male mice, GCaMP6f 4 2-3 months old male mice, SCH 23390 31 2-3 months old male mice, M4-DREAAD, 21 2-3 months old male mice, 6-OHDA lesion 8 2-3 months mice, Arch 15 2-3 months old male mice and ChR2 19 2-3 months male mice.

Stereotactic surgery for viral/toxin injections and cannula/light fiber implantation

Male mice 2-4 months old were deeply anaesthetized with isoflurane (5%, Abbot Laboratories) and placed in a stereotaxic frame (Kopf). Anesthesia was kept constant with 1.5 – 2% isoflurane supplied per anesthesia nosepiece and body temperature maintained at 36°C with a heating pad controlled by rectal thermometer (DC temperature controller). After injecting 0.1 ml of Lidocaine under the skin as analgesia, the skull was exposed and perforated with a stereotaxic drill at the desired coordinates relative to Bregma (Franklin & Paxinos 2007). For postoperative care, mice were supplied with drinking water containing 250mg/l Carprofen (Rimadyl, Pfizer) and 400 mg/l Enrofloxacin (Baytril, KVP pharma) for 14 days.

For optogenetic fibre implantation, one optic cannula (Doric lenses, 200-400 μm, 0.53NA) per mouse was implanted 0.5mm over the ventral PAG (AP = -4.5, ML = 0, DV = -2.7) for optogenetic manipulations. Placing a single fiber at midline ensured bilateral illumination of

vPdRD neurons, which accumulate close to the midline under the 3rd ventricle.vPAG/DR (Supplementary Fig. 7c-d). Two guide cannulas (Bilaney, C316GS-4/SPC) were implanted bilaterally 0.5 mm over the CEl (AP = -4.5, ML = 0, DV = -2.7) for drug infusions. Both were fixed on the skull with dental cement (SuperBond C&B kit, Prestige Dental Products).

Micro4 Micro Syringe Pump controller (World Precision Instruments) was used to regulate injection volumes with a rate of 10 nl/min. The glass needle was left in place for 5 minutes after the injection volume was delivered. A detailed list of viral constructs is provided in Supplementary Fig. 15a.

Histological analysis

To verify virus expression (see Supplementary Fig.15a) and correct locations of optical fiber tips and cannulae, animals were sacrificed by a mixture of 10mg/ml Ketamine (OGRIS Pharma) and 1 mg/ml Medetomidine hydrochloride (Domitor, ORION Pharma) in 1 x PBS and tissue sectioning was performed as described under section 'Immunohistochemistry'. Expression of viral constructs and location of optical fiber tips/ cannulae were assessed for correct targeting (Supplementary Fig. 4, 7).

Fear Conditioning

Mice were handled on two different days prior to all behavioral training experiments. Fear Conditioning was separated into habituation, conditioning and testing phase and conducted on three different consequent days in a large sound-proof isolation cubicle that contained an adaptive mouse test cage (Coulbourn instruments). The context of the mouse test cage was modified to make the box distinct for different phases of the experiment. *Conditioning:* (Context A) the mouse test cage was adapted by a grey/white striped box formed on basis of a symmetric trapeze (15 x 12 x 7 cm), the floor texture consisted of the characteristic shock grid baseplate, box walls were swiped with lemon flavor. *Testing:* (Context B) test cage was adapted by a square white box, the floor consisted of a white flat baseplate, box walls were swiped with ethanol flavor. On day 1, mice individually underwent habituation phase in context B with each session taking 300 s. On day 2, mice were conditioned individually in context A with 4 pure tones (3 kHz, 70 dB, 20 s each) delivered at intervals with variable duration (80-120 s), each sound co-terminating with a 1 s, 0.5 mA foot shock, delivered by a precision regulated animal shocker H13-15 (Coulbourn Instruments). Testing of fear memory was performed 24h after conditioning on day 3 in context B by recording behavioral responses to 4 pure tones (3kHz, 70 dB, 20s each) delivered at variable intervals (80-120s). Matlab scripts were programmed to deliver foot shocks and tones. The isolation cubicle was illuminated in every phase of the experiment and the behavior was captured with a CCD camera at 25 fps and stored on PC. Test cages and test floors were thoroughly cleaned with water and dedicated flavor-alcohol mixtures in between mouse runs on a given day. Behavioral responses of all phases were analyzed off line by Ethovision software or visually by an observer blind to the experimental condition. A list of behavioral experiments and the experimental history of different cohorts is provided in Supplementary Fig. 15b.

Blocking experiment

The blocking experiment was performed as described earlier [25] with some modifications. The preparations and equipment were identical to fear conditioning (described above), but based on a different protocol (Figure 4). All blocking experiment phases took place in the dark without constant illumination. After Habituation phase on day 1 (identical as described in Fear Conditioning above), mice underwent three consecutive days of conditioning in context A on day 2 to day 4, each day consisting of a session where 30 s periods of 1 s house light pulses (CS A) at 1 Hz were presented 4 times, each period co-terminating with a 1s, 0.5 mA foot shock. The interval between these periods randomly varied from 80 to 120 s. Conditioning phase was followed by a two-day compound conditioning phase on day 5 and 6, again in context A, where animals received 4 times a compound CS on each session/day, composed of CS A accompanied by 1 Hz pulsed white noise (CS B) in random 80-120 s intervals, each presentation co-terminating with one 0.5 mA foot shock. The next day (day 7), behavioral responses to 12 CS A and 12 CS B presentations were recorded in one session. The CS presentation in this testing phase was designed in a way that two CSA were followed by two CSB, with a constant time interval of 60s between each CS (CSA-60s-CSA-60s-CSB-60s-CSB-…)

Systemic injections in behavioral experiments

For neuronal modulation of animals expressing DREADDs, Clozapine N-oxide (Sigma, 2.5mg/kg) was diluted in physiological 1xPBS and injected intraperitoneally 30 min before the start of the experimental session. Animals that received this treatment in experiments were habituated by PBS injections during handling sessions.

Optogenetic manipulation in behavioral experiments

Animals that had undergone stereotactic injection of optogenetic AAV virus for later neuronal modulation during behavior underwent habituation for attaching a fiber-optic patch cord (doric lenses) on implanted opto fibers. For ChR2 activation, laser trains of blue light (473nm) were delivered consisting 20 ms pulses delivered at 20 Hz (if not noted otherwise) at an intensity of 8-10 mW at the fiber tip. For Arch activation, laser trains of constant yellow light (568nm) were delivered at an intensity of 5-7 mW. Intensity of all laser stimulations were measured before every experiment at the tip of the optic fiber via Power Meter (Thorlabs, PM100D). Laser stimulation was controlled by MatLab scripts during conditioning experiments and by Arduino boards running customized scripts executed by any-maze software (Stoelting) during pain tests and baseline anxiety tests.

Intracranial drug delivery during behavioral experiments

Intracerebral drug administration was delivered through previously (2-4 weeks) implanted guide cannulas. Animals were handled once a day 5 min for 3 days. On day of the experiment, internal cannulas that protruded 1 mm beyond the edge of the guide cannula were inserted and either D1 receptor antagonist SCH23390 (Tocris) in saline or saline vehicle were infused bilaterally. 80ng doses of SCH23390 in 0.2 μl saline or saline alone were injected (0.2μl/side) over a period of 5 min using a syringe controlled by an infusion pump (Harvard Apparatus Pump 11). Behavioral tests were started 30 min after infusion.

Automated von Frey test

Touch sensitivity was tested with a dynamic plantar aesthesiometer (Ugo Basile S.R.L., Italy). Mice were habituated to the testing chambers for approx. 2 hours prior to testing. Then each hindpaw was tested 3 times with an increased force ranging from 0 to 10g with a 20sec ramp up time and at least 20sec between each trial on the same mouse. The average of 3 trials was calculated for each hindpaw. Read-out parameters were the force and latency at which the mouse lifted the hindpaw.

Hot plate test

Thermal sensitivity was tested 1 week after von Frey testing using a hot plate analgesia meter (IITC Life Science Inc., CA, USA). Mice were put on the hot plate at 45 °C and the temperature was increased from 45 to 55 °C within 2 minutes. The experiment was stopped as soon as the mice performed the first jump. Mice were videotaped and the latency and temperature of the first reaction (hindpaw shaking or licking) or jump recorded.

Elevated plus maze

Mice were placed in the center zone (6.5 x 6.5cm), facing an open arm of a custom-built elevated plus maze (elevated 54cm above the floor) with 2 open arms (OA, 30cm length, 7cm width) and 2 wall-enclosed arms (closed arms, CA, 30cm length, 6cm width, walls 14.5cm high) and let explore freely for 5 minutes. Their path was videotracked using Topscan software (Cleversys, Inc., VA, USA) and the amount of time spent and distance travelled in the open arms, closed arms and center zone were evaluated.

Light/Dark box

Mice were placed in the light zone and let explore the Light/Dark arena (open field arena from TSE-Systems modified with custom-built dark zone boxes) freely for 20 minutes. Their path was videotracked in the light zone using Videomot 2 software (V7.X, TSE-Systems GmbH, Germany) and the amount of time spent in the light versus dark zones and distance travelled in the light zone were evaluated, as well as the latency until they escaped to the dark zone. Lux levels were 150 lux in the light zone and about 0 lux in the dark zone. Each zone (light zone and dark zone) was 24.5cm x 50cm in size.

Microdialysis

Experiments were performed by Brains-OnLine (Charles River Laboratories) following established amygdala microdialysis routines for awake behaving animals. Adult male rats were anesthetized using isoflurane (2%, 800 mL/min O2). Bupivacaine/epinephrine was used for local analgesia and carprofen was used for peri-/post-operative analgesia. The animals were placed in a stereotaxic frame (Kopf instruments, USA). Rats were implanted with a push-pull microdialysis probe (2 mm exposed surface, PEE membrane, BrainLink, the Netherlands) in the amygdala (AP = -3.3, ML = -4.5, DV = -9). Note that the stereotaxic position between BLA and posterior CE (Supplementary Fig. 5a) and the use of lateral exposed dialysis surfaces allows for sampling BLA and CE DA while preventing excessive CE tissue damage. After surgery, animals were housed individually in cages and provided food and water ad libitum. Microdialysis sampling was initiated approximately 24 hours

after surgery. On the days of the sampling (Days 1and 2), the probes were connected with PAN tubing to a microperfusion pump (Harvard PHD 2000 Syringe pump, Holliston, MA or similar). Microdialysis probes were perfused with aCSF containing 147 mM NaCl, 3.0 mM KCl, 1.2 mM CaCl2 and 1.2 mM MgCl2, at a flow rate of 1.5 μL/min. Microdialysis samples were collected for 15-minute periods by an automated fraction collector (820 Microsampler, Univentor, Malta) into polystyrene (300 μl) mini-vials. All the dialysis samples were stored at -80°C for later analysis. After habituation, 15 minutes samples of baseline dialysate were collected for 90 minutes in the animals' home cage. Rats were then placed inside the test cages with grid floor shockers (Coulbourn Instruments, Lehigh Valley, PA) and dialysate samples were collected 1 hour before 2 shocks were administered (2x 1 sec shocks at 0.6 mA). Animals remained in the test cage for 30 minutes before being moved back to their home cages for the remainder of the experiment. The next day, animals underwent the same procedure as on day 1 except that the foot shock was omitted. After microdialysis, brains were fixed in 4 % PFA. Histological samples were visually inspected for correct probe placement.

Deep brain Ca^{2+} Imaging

Deep brain calcium imaging was conducted using the nVista HD 2.0 system (In Vivo Rodent Brain Imaging System, Inscopix, Inc). A microendoscope was implanted directly above the ventral PAG and a baseplate (BPL-2) was attached to the skull with dental cement 1 week later. Mice were habituated to camera mounting the day before the experiment. On experimental day, the microscope was attached to the baseplate before the start of the behavioral experiment. Ca^{2+} signals during behavioral testing were imaged with nVistaHD v2.0.32 at 20fps. We compensated for movement during video acquisition using custom ImageJ scripts and Mosaic v1.2 (Inscopix, Inc) software. The video was further analyzed in Mosaic analysis suite v1.2, first by applying a ΔF/F0 normalization, where F0 was based on the entire length of the movie. Bulk signals were derived from the entire field of view and low-pass filtered at 0.5 Hz. Traces of individual units were extracted by principal/ independent component analysis (PCA/ICA) and low-pass filtered at 0.5 Hz and manually sorted. Ca^{2+} events were detected automatically whenever the rise in the Ca^{2+} traces exceeded and amplitude of 3 SD and a τ of 0.5 s.

All further analysis was performed in Neuroexplorer software (Plexon Inc.) and Python scripts. Cells were classified as responders when their event counts during a 4s time window at CS and/or US presentation exceeded the > 95 % confidence interval for the expected mean firing rate. Bulk signals and unit traces were binned at 0.5-2 s, represented as population means and analyzed using parametric statistics throughout.

Immunohistochemistry

Animals were deeply anaesthetized with a mixture of 10mg/ml Ketamine (OGRIS Pharma) and 1mg/ml Medetomidine hydrochloride (Domitor, ORION Pharma) in 1xPBS and transcardially perfused with 10ml of cold 1xPBS followed by 25ml of 4% (PFA) in 1xPBS. Brains were immediately removed, postfixed in 4% PFA at 4°C overnight and transferred to 1xPBS at 4°C. 70-100μm vibratome sections were cut and transferred in PBS-T (1xPBS plus 0.1% Triton X-100). Non-specific binding was blocked with 1% BSA/ 2%NGS in PBS-T for

2 hours. Primary antibodies (goat anti SST (sc-7819; Santa Cruz; for amygdala SST[+] neurons51), mouse anti-PKC-δ (610398; BD Biosciences; for amygdala PKCδ[+] neurons4), chicken anti-TH (AB9702; Millipore; for midbrain TH[+] neurons52) were diluted 1:500 – 1:1000 in blocking solution and incubated for 24h at 4°C. Standard secondary antibodies (Invitrogen) in blocking solution were incubated for 2h at room temperature, sections mounted with Fluoromount G (SouthernBiotech) and viewed under a Leica stereomicroscope and a Zeiss LSM 710 Spectral confocal microscope.

To identify recorded cells after acute brain slice electrophysiology, internal solution for patch-clamp recording contained 0.1% w/v biocytin (Sigma). Slices were transferred to 4% PFA in 1xPBS after recording and stained as described above including Fluorophore tagged Streptavidin (Sigma) to secondary antibody incubation.

Verification of M3-DREADD and M4-DREADD virus expression (both tagged with mCherry fluorophore) in behavior experiments that included the DREADD system was optimized with IHC against tdtomato as described above with anti-DsRed polyclonal antibody (Living Colors).

Combined CTB tracing/TH IHC experiments

CTB-Alexa Fluor 555 (Invitrogen) was delivered by stereotaxic injection. Animals were sacrificed 1 week after injection and brains processed for IHC as described above. Co-localization of CTB back-labelled neurons with either PKCδ (CEl) or TH (PAG) labelling was scored by an observer blind to the experimental condition.

6-OHDA vPAG lesions

6-Hydroxydopamine Hydrobromide (Sigma) in saline containing 0.01% (w/v) ascorbic acid, was delivered by two stereotaxic 100nl injections into the rostral and caudal ventral PAG region at a concentration of 10μg/μl.

D1R Knockdown

To suppress D1R expression in the CEl we constructed an AAV-based vector expressing GFP and miRNA-adapted shRNAs in the optimized miR-E backbone53 under control of the SFFV promoter (AAV-SFFV-GFP-miR; ASGE). Two independent shRNAs targeting D1R (guide sequences: 5'-TAGTA…[add 22mer guides]) were designed based on optimized design rules, cloned into miR-E and tested for knockdown potency at the protein level using an established two-color reporter assay53. In brief, NIH-3T3 cells were stably transfected with a construct expressing a td-Tomato transgene harboring target sites of D1R and several control shRNAs in its 3'UTR (name vector). Subsequently, cells were transduced with ASGE vectors harboring D1R and control shRNAs, and td-Tomato reporter knockdown in GFP-shRNA expressing cells was quantified using flow cytometry. Percentage of knockdown was calculated as a ratio of the mean td Tomato signal in the GFP positive cell population to the mean td Tomato signal in the GFP negative cell population using the formula as follows:

$$\% \ knockdown = 100 - \frac{mean \ tdTomato \ GFP \ pos}{mean \ tdTomato \ GFP \ neg} * 100$$

Fiber density analysis

Transgenic SST::Cre and PKCδ::Cre mice received CEl targeted injections of AAV::ChR2-YFP. Brains were perfused, cut by vibratome and slices immunostained against TH to confirm correct targeting to the vPAG/DR region. The analysis was performed using Definiens Developer XD software on Maximum Intensity Projections of the 3D datasets. To segment the axons a 2D Bandpass Filter was applied and the resulting Image was thresholded. Objects low in contrast were removed and the total area of axons per image was measured.

Acute brain slice electrophysiology

Virally infected TH::Cre, SST::Cre and PKCδ::Cre single or double transgenic male mice (2 - 3 months old) were deeply anesthetized with Isoflurane, decapitated and their brains quickly chilled in sucrose-based dissection buffer, bubbled with 95% O_2/5% CO_2 containing the following (in mM): 220 Sucrose, 26 $NaHCO_3$, 2.4 KCl, 10 $MgSO_4$, 0.5 $CaCl_2$, 3 Sodium Pyruvate, 5 Sodium Ascorbate and 10 glucose54. Transverse coronal brain slices (300 μm) were cut in dissection buffer using a Vibratome (Leica, VT1000S) and immediately incubated for 15 min recovery phase in oxygenated artificial cerebrospinal fluid (aCSF) 126 NaCl, 2.5 KCl, 1.25 NaH2PO4, 26 NaHCO3, 2.5 CaCl2, 2.5 MgCl2, and 25 glucose in 95% O2/5% CO2 at 32°C. This was followed by a slice resting phase with oxygenated aCSF for at least 45 min at room temperature (RT).

Individual brain slices containing CEl were placed on the stage of an upright, infrared-differential interference contrast microscope (Olympus BX50WI) mounted on a X-Y table (Olympus) and visualized with a 40x water immersion objective by an infrared sensitive digital camera (Hamamatsu, ORCA-03). Slices were fully submerged and continuously perfused at a rate of 1-2 ml per min with oxygenated aCSF.

Optogenetic circuit mapping

PKCδ[+] and SST^{+} neurons in the CEl were identified by the presence of GFP fluorescence. Patch pipettes were pulled on a Flaming/Brown micropipette puller (Sutter, P-97) from borosilicate glass (1.5 mm outer and 0.86 mm inner diameter, Sutter) to final resistances ranging from 3 to 5MΩ. Internal solution for voltage-clamp recordings of responses to optogenetic stimulation contained (in mM): 135 Cesium Methanesulfonate, 5 KCl, 10 HEPES, 2 $MgCl_2$, 0.2 EGTA, 1 Na_2ATP, 0.4 NaGTP, 10 Na_2Phosphocreatine for excitatory responses in the CEl and 140 KCL, 10 HEPES, 2 $MgCl_2$, 0.2 EGTA, 1 Na_2ATP, 0.4 NaGTP, 10 Na_2Phosphocreatine for inhibitory responses in the PAG (280-290 mOsmol). Membrane currents were recorded with a Multiclamp 700B amplifier (Molecular Devices). Electrophysiological signals were low pass filtered at 3kHz, sampled at 10 kHz (Digidata 1440A, Axon Instruments) and stored on a PC for offline analysis with pClamp 10 software (Molecular Devices).

Cells were held at -70 mV. Cells were allowed to reestablish constant activity during 5 minutes waiting time after breaking the seal. Twenty ms blue light pulses were delivered through a 40x electrophysiology microscope objective, driven by a 120W mercury lamp (X-Cite 120 PC Q). The amplitude of 4 pulses, 5 seconds apart, was averaged as postsynaptic response. Inhibitory responses were identified by adding 10 μM Bicuculline, excitatory responses by adding 10 μM CNQX + 50 μM D-APV (all Sigma) to the bath.

LTP experiments

Standard procedures were applied to prepare coronal slices from male C57Bl/6J mice (P28-P47). In brief, mice were deeply anaesthetized by inhalation of 4% isoflurane and killed by decapitation. A block of tissue containing the amygdala was rapidly removed and placed in a dissection buffer containing (mM): Sucrose 195; KCl, 2.4; NaH_2PO_4, 1.25; $NaHCO_3$, 24; $MgSO_4$, 10; $CaCl_2$, 0.5; glucose, 10; bubbled with 95% O_2/ 5% CO_2. Either, 400 μm coronal slices (field potential recordings) or 300 μm coronal slices (patch-clamp recordings) were prepared on a vibratome (Model 1000, The Vibratome Company, St. Louis, USA). Whole cell patch-clamp recordings of excitatory postsynaptic currents (EPSCs) were recorded in a submerged chamber with a patch-clamp amplifier (EPC-9, Heka, Lamprecht, Germany) at $30 \pm 1°C$. Standard artificial cerebrospinal fluid (aCSF) was composed of (in mM): NaCl, 119; KCl, 2.5; NaH_2PO_4, 1.25; $NaHCO_3$, 26; $MgSO_4$, 1; $CaCl_2$, 2; glucose, 20; bubbled with 95% O_2/5% CO_2. Picrotoxin (50 μM) was added to block $GABA_A$ receptors. Patch pipettes were pulled from borosilicate glass (GC150TF-10, Clark Electromedical Instruments, Pangbourne, UK) to resistances of 3 MΩ, and filled with (in mM): potassium gluconate, 135; KCl, 5; Hepes, 10; $MgCl_2$, 2; EGTA, 0.2; MgATP, 4; Na_3GTP, 0.4; K_3-phosphocreatine, 10; biocytin, 0.1; pH 7.2 (with KOH). A liquid junction potential of +10 mV of the pipette solution was corrected for. After obtaining the whole cell configuration, neurons were held at -70 mV. Electrodes were positioned as indicated for local field potentials. EPSCs were evoked every 15 s with stimulus intensities adjusted to generate EPSC amplitudes of approximately 150 pA. Peak current amplitudes of EPSCs were calculated by averaging four consecutive responses. LTP was induced by two trains of 100 Hz/1s separated by 20 s, paired with postsynaptic depolarization to –10 mV in voltage clamp mode. LTP was quantified by normalizing and averaging maximal EPSC amplitudes during the last 5 min of experiments (i.e. 30 min after LTP induction) relative to 10 min baseline. Recordings with changes in access resistance above 25% were discarded.

Local field potential recordings were conducted in an interface chamber at 32 °C ± 1 °C. aCSF was composed of (in mM): NaCl, 125; KCl, 2.5; NaH_2PO_4, 0.8; $NaHCO_3$, 25; $MgCl_2$, 1; $CaCl_2$, 2; glucose, 10; bubbled with 95% O_2/ 5% CO_2. Gabazine (0.1 μM) was added to reduce GABAergic inhibition. Recording pipettes were pulled from borosilicate glass (GC150TF-10, Clark Electromedical Instruments, Pangbourne, UK), filled with aCSF and sited at the lateral central amygdala. A concentric bipolar electrode (FHC Inc, Bowdoin, ME, USA) was positioned on the surface of the slice above the basal amygdala at the border to the capsular central amygdala. Field potentials were evoked by stimuli of 100 μs duration delivered by a stimulus isolator (Isoflex, AMPI, Jerusalem, Israel) at 0.016 Hz. Stimulus intensity was adjusted to evoke halfmaximal responses. Signals were amplified by a DAM-80 amplifier (WPI, Berlin, Germany) and digitized with a CED 1401plus interface

(Cambridge Electronic Design, Cambridge, U.K). Signal amplitude was measured as the sum of the difference between onset and peak of the negative voltage deflection, and the difference of the peak of the negative voltage deflection and the succeeding positive peak, divided by two. To induce LTP, a high-frequency stimulation pattern (HFS) consisting of three trains of 100 stimuli at 100 Hz separated by 30 s was executed at time point zero. LTP was quantified by normalizing and averaging field potentials during the last 5 min of experiments (i.e. 55 - 60 min after LTP induction) relative to 30 min baseline. To verify significant differences induced by pharmacological manipulations, averaged field potential amplitudes during the last 5 min of recordings were compared.

Experience dependent synaptic plasticity

To evaluate experience dependent synaptic plasticity in the CEl, the male 6 OHDA lesioned and D1R Knock down cohort were sacrificed immediately after the fear testing step of our fear conditioning protocol and coronal slices prepared as described above. To obtain comparisons of the synaptic strength of BLA inputs onto SST^+ and PKC-δ^+ neurons, we performed subsequent whole-cell patch-clamp recordings of pairs of different neuronal subtypes next to each other (<60μm) to avoid an error due to different distances to the stimulation electrode. The Index of each pair as shown in the data represents the difference of the response amplitude to BLA electric stimulation in voltage clamp of a given pair of one SST^+ and one PKC-δ^+ neuron, divided by the sum of the same values.

Neuronal population sequencing

Amygdala punches (1 mm diameter, 300 μm thickness) of 6 week old males from PKCδ::Cre or SST::Cre animals crossed to Cre-dependent Rosa::td-Tomato lines were enzymatically dissociated and FACS sorted for approximately 103 td-Tomato$^+$ cells. SMARTer® smRNA-Seq Kit for Illumina® (Clontech, 78100 Saint-Germain-en-Laye, France) prepared libraries were submitted to deep sequencing on a HiSeq 2500 system (Illumina, San Diego, USA). The reads were mapped to the Mus musculus mm10 reference genome either with STAR (version 2.4.0d)55 or TopHat (version 2.0.9)56. Reads aligning to rRNA sequences were filtered out prior to mapping. The read counts for each gene were detected using HTSeq (version 0.5.4p3)57. The counts were normalized using the TMM normalization from edgeR package in R. Prior to statistical testing the data was voom transformed and then the differential expression between the sample groups was calculated with limma package in R. The functional analyses were done using the topGO and gage packages in R. Complete data will be published elsewhere.

Sample sizes

No statistical methods were used to predetermine sample sizes. Sample size were similar as reported in previous publications4,30,58,59.

Randomization

All animals and samples were randomly assigned to the experimental groups. Experimental conditions (Training and testing contexts, stimulus types) were fixed. Stimulus timing (CS, US) was applied in pseudorandom time intervals.

Blinding

Data collection and analysis were not performed blind to the conditions of the experiments. Data was acquired, processed and analyzed by automated workflows, except Fig. 1e, f, Supplementary Fig. 3a, Supplementary Fig. 4a,b, Supplementary Fig. 5a,b, Supplementary Fig. 7a,b,c,d, Supplementary Fig. 10e, Supplementary Fig. 11b.

Statistics

All statistics were performed in Graph Pad Prism ® (Version 6), unless otherwise indicated, and all statistical tests used are indicated in the figures legends. Experimental designs with one categorical independent variable (Fig. 1e,l, Fig. 3f, Fig. 5e, Supplementary Fig. 10c, Supplementary Fig. 11d) were assessed by Shapiro-Wilk normality tests. When normality test passed, parametric statistics (t-test, one-way ANOVA) were applied. In case of non-normal distributions, non-parametric statics (Mann-Whitney U-test and Wilcoxon Signed Rank test) were planned. Experimental designs with two categorical independent variables (Fig. 2c-g, Fig. 3b,d,h, Fig. 4e,g,j, Fig. 5b,c,d, Supplementary Fig. 3b, Supplementary Fig. 8a-h, Supplementary Fig. 13a,b, Supplementary Fig. 10f) were assumed to be normal and analyzed by two-way ANOVA without formally testing normality. All significance levels are given as two-sided and were corrected for multiple comparisons, wherever applicable. Omnibus significance values were rounded up for values $P < 0.0001$. Post-hoc significance values were rounded up and given as * for values $P < 0.05$, ** for values $P < 0.01$, *** for values $P < 0.001$ and **** for values $P < 0.0001$; where no significance was made explicit, the test did not reach a significance level of $P < 0.05$.

Data exclusion

For slice electrophysiology approximately 10 out 50 animals did not reach sufficient virus expression and/or missed injection targets and were excluded. Out of the SCH 23390 cohort, 9 out of 31 animals were excluded from the analysis due to misplaced or blocked infusion cannulae.

Code availability

The code for analysis is available from the corresponding author upon reasonable request.

Data availability

The data that support the findings of this study (Fig. 1-5, Supplementary Figs. 3-5 and Supplementary Figs. 7-13) are available from the corresponding author upon reasonable request. Data Supporting Supplementary Figs. 1 & 2 are from Allen Mouse Brain Connectivity Atlas (http://connectivity.brain-map.org/). For data Supporting Supplementary Fig. 6 see Accession Codes section.

For additional information please refer to the corresponding Life Sciences Reporting Summary.

Supplementary Material

Refer to Web version on PubMed Central for supplementary material.

Acknowledgements

References

1. LeDoux J. The amygdala. Current biology : CB. 2007; 17:R868–874. DOI: 10.1016/j.cub. 2007.08.005 [PubMed: 17956742]

2. Gallistel CR, Matzel LD. The neuroscience of learning: beyond the Hebbian synapse. Annual review of psychology. 2013; 64:169–200. DOI: 10.1146/annurev-psych-113011-143807

3. Ciocchi S, et al. Encoding of conditioned fear in central amygdala inhibitory circuits. Nature. 2010; 468:277–282. DOI: 10.1038/nature09559 [PubMed: 21068837]

4. Haubensak W, et al. Genetic dissection of an amygdala microcircuit that gates conditioned fear. Nature. 2010; 468:270–276. nature09553 [pii]. DOI: 10.1038/nature09553 [PubMed: 21068836]

5. Li H, et al. Experience-dependent modification of a central amygdala fear circuit. Nature neuroscience. 2013; 16:332–339. DOI: 10.1038/nn.3322 [PubMed: 23354330]

6. Cui Y, et al. A Central Amygdala-Substantia Innominata Neural Circuitry Encodes Aversive Reinforcement Signals. Cell reports. 2017; 21:1770–1782. DOI: 10.1016/j.celrep.2017.10.062 [PubMed: 29141212]

7. Cassenaer S, Laurent G. Conditional modulation of spike-timing-dependent plasticity for olfactory learning. Nature. 2012; 482:47–52. DOI: 10.1038/nature10776 [PubMed: 22278062]

8. Schultz W. Behavioral dopamine signals. Trends in neurosciences. 2007; 30:203–210. DOI: 10.1016/j.tins.2007.03.007 [PubMed: 17400301]

9. Fiorillo CD. Two dimensions of value: dopamine neurons represent reward but not aversiveness. Science. 2013; 341:546–549. DOI: 10.1126/science.1238699 [PubMed: 23908236]

10. Cohen J, Haesler S, Vong L, Lowell B, Uchida N. Neuron-type-specific signals for reward and punishment in the ventral tegmental area. Nature. 2012; 482:85–88. DOI: 10.1038/nature10754 [PubMed: 22258508]

11. Hart AS, Rutledge RB, Glimcher PW, Phillips PE. Phasic dopamine release in the rat nucleus accumbens symmetrically encodes a reward prediction error term. The Journal of neuroscience : the official journal of the Society for Neuroscience. 2014; 34:698–704. DOI: 10.1523/ JNEUROSCI.2489-13.2014 [PubMed: 24431428]

12. Bromberg-Martin E, Matsumoto M, Hikosaka O. Dopamine in motivational control: rewarding, aversive, and alerting. Neuron. 2010; 68:815–834. DOI: 10.1016/j.neuron.2010.11.022 [PubMed: 21144997]

13. Silberman Y, Winder DG. Corticotropin releasing factor and catecholamines enhance glutamatergic neurotransmission in the lateral subdivision of the central amygdala. Neuropharmacology. 2013; 70:316–323. DOI: 10.1016/j.neuropharm.2013.02.014 [PubMed: 23470280]

14. Naylor J, et al. Dopamine attenuates evoked inhibitory synaptic currents in central amygdala neurons. The European journal of neuroscience. 2010; 32:1836–1842. DOI: 10.1111/j. 1460-9568.2010.07457.x [PubMed: 20955472]

15. Brischoux F, Chakraborty S, Brierley DI, Ungless MA. Phasic excitation of dopamine neurons in ventral VTA by noxious stimuli. Proceedings of the National Academy of Sciences of the United States of America. 2009; 106:4894–4899. DOI: 10.1073/pnas.0811507106 [PubMed: 19261850]

16. Ungless MA, Magill PJ, Bolam JP. Uniform inhibition of dopamine neurons in the ventral tegmental area by aversive stimuli. Science. 2004; 303:2040–2042. DOI: 10.1126/science.1093360 [PubMed: 15044807]

17. Tan K, et al. GABA neurons of the VTA drive conditioned place aversion. Neuron. 2012; 73:1173–1183. DOI: 10.1016/j.neuron.2012.02.015 [PubMed: 22445344]

18. Mileykovskiy B, Morales M. Duration of inhibition of ventral tegmental area dopamine neurons encodes a level of conditioned fear. The Journal of neuroscience : the official journal of the Society for Neuroscience. 2011; 31:7471–7476. DOI: 10.1523/JNEUROSCI.5731-10.2011 [PubMed: 21593330]

19. Schultz W. Neuronal Reward and Decision Signals: From Theories to Data. Physiological reviews. 2015; 95:853–951. DOI: 10.1152/physrev.00023.2014 [PubMed: 26109341]

20. Dougalis A, et al. Functional properties of dopamine neurons and co-expression of vasoactive intestinal polypeptide in the dorsal raphe nucleus and ventro-lateral periaqueductal grey. The European journal of neuroscience. 2012; 36:3322–3332. DOI: 10.1111/j.1460-9568.2012.08255.x [PubMed: 22925150]

21. Matthews GA, et al. Dorsal Raphe Dopamine Neurons Represent the Experience of Social Isolation. Cell. 2016; 164:617–631. DOI: 10.1016/j.cell.2015.12.040 [PubMed: 26871628]

22. Lu J, Jhou TC, Saper CB. Identification of wake-active dopaminergic neurons in the ventral periaqueductal gray matter. The Journal of neuroscience : the official journal of the Society for Neuroscience. 2006; 26:193–202. DOI: 10.1523/JNEUROSCI.2244-05.2006 [PubMed: 16399687]

23. McDevitt RA, et al. Serotonergic versus nonserotonergic dorsal raphe projection neurons: differential participation in reward circuitry. Cell reports. 2014; 8:1857–1869. DOI: 10.1016/j.celrep.2014.08.037 [PubMed: 25242321]

24. Fibiger HC, LePiane FG, Jakubovic A, Phillips AG. The role of dopamine in intracranial self-stimulation of the ventral tegmental area. The Journal of neuroscience : the official journal of the Society for Neuroscience. 1987; 7:3888–3896. [PubMed: 3121802]

25. McNally G, Cole S. Opioid receptors in the midbrain periaqueductal gray regulate prediction errors during pavlovian fear conditioning. Behavioral neuroscience. 2006; 120:313–323. DOI: 10.1037/0735-7044.120.2.313 [PubMed: 16719696]

26. Johansen JP, Tarpley JW, LeDoux JE, Blair HT. Neural substrates for expectation-modulated fear learning in the amygdala and periaqueductal gray. Nature neuroscience. 2010; 13:979–986. DOI: 10.1038/nn.2594 [PubMed: 20601946]

27. de la Mora MP, Gallegos-Cari A, Arizmendi-Garcia Y, Marcellino D, Fuxe K. Role of dopamine receptor mechanisms in the amygdaloid modulation of fear and anxiety: Structural and functional analysis. Prog Neurobiol. 2010; 90:198–216. DOI: 10.1016/j.pneurobio.2009.10.010 [PubMed: 19853006]

28. Swanson LW. The projections of the ventral tegmental area and adjacent regions: a combined fluorescent retrograde tracer and immunofluorescence study in the rat. Brain research bulletin. 1982; 9:321–353. [PubMed: 6816390]

29. Lee H, Wheeler D, Holland P. Interactions between amygdala central nucleus and the ventral tegmental area in the acquisition of conditioned cue-directed behavior in rats. The European journal of neuroscience. 2011; 33:1876–1884. DOI: 10.1111/j.1460-9568.2011.07680.x [PubMed: 21488988]

30. Edelmann E, Lessmann V. Dopamine regulates intrinsic excitability thereby gating successful induction of spike timing-dependent plasticity in CA1 of the hippocampus. Frontiers in neuroscience. 2013; 7:25.doi: 10.3389/fnins.2013.00025 [PubMed: 23508132]

31. Yu K, Garcia da Silva P, Albeanu DF, Li B. Central Amygdala Somatostatin Neurons Gate Passive and Active Defensive Behaviors. The Journal of neuroscience : the official journal of the Society for Neuroscience. 2016; 36:6488–6496. DOI: 10.1523/JNEUROSCI.4419-15.2016 [PubMed: 27307236]

32. Nagatsu I, Karasawa N, Kondo Y, Inagaki S. Immunocytochemical localization of tyrosine hydroxylase, dopamine-beta-hydroxylase and phenylethanolamine-N-methyltransferase in the adrenal glands of the frog and rat by a peroxidase-antiperoxidase method. Histochemistry. 1979; 64:131–144. [PubMed: 43302]

33. Roy M, et al. Representation of aversive prediction errors in the human periaqueductal gray. Nature neuroscience. 2014; 17:1607–1612. DOI: 10.1038/nn.3832 [PubMed: 25282614]

34. Correia PA, et al. Transient inhibition and long-term facilitation of locomotion by phasic optogenetic activation of serotonin neurons. eLife. 2017; 6doi: 10.7554/eLife.20975

35. Kamin LJ. Punishment and aversive behavior. CampbellChurch RM, editorsAppleton-Century-Crofts; 1969. 279–296.

36. Di Scala G, Mana MJ, Jacobs WJ, Phillips AG. Evidence of Pavlovian conditioned fear following electrical stimulation of the periaqueductal grey in the rat. Physiology & behavior. 1987; 40:55–63. [PubMed: 3615655]

37. McNally GP, Johansen JP, Blair HT. Placing prediction into the fear circuit. Trends in neurosciences. 2011; 34:283–292. DOI: 10.1016/j.tins.2011.03.005 [PubMed: 21549434]

38. Ozawa T, et al. A feedback neural circuit for calibrating aversive memory strength. Nature neuroscience. 2016; doi: 10.1038/nn.4439

39. Rescorla RA, Wagner AR. A theory of Pavlovian conditioning: variations in the effectiveness of reinforcement and nonreinforcement. Appleton-Century-Crofts; 1972. 64–99.

40. Pearce JM, Hall G. A model for Pavlovian learning: variations in the effectiveness of conditioned but not of unconditioned stimuli. Psychological review. 1980; 87:532–552. [PubMed: 7443916]

41. Venniro M, et al. The Anterior Insular Cortex-->Central Amygdala Glutamatergic Pathway Is Critical to Relapse after Contingency Management. Neuron. 2017; 96:414–427 e418. DOI: 10.1016/j.neuron.2017.09.024 [PubMed: 29024664]

42. Fadok JP, Dickerson TM, Palmiter RD. Dopamine is necessary for cue-dependent fear conditioning. The Journal of neuroscience : the official journal of the Society for Neuroscience. 2009; 29:11089–11097. DOI: 10.1523/JNEUROSCI.1616-09.2009 [PubMed: 19741115]

43. De Bundel D, et al. Dopamine D2 receptors gate generalization of conditioned threat responses through mTORC1 signaling in the extended amygdala. Molecular psychiatry. 2016; 21:1545–1553. DOI: 10.1038/mp.2015.210 [PubMed: 26782052]

44. Kim J, Zhang X, Muralidhar S, LeBlanc SA, Tonegawa S. Basolateral to Central Amygdala Neural Circuits for Appetitive Behaviors. Neuron. 2017; 93:1464–1479 e1465. DOI: 10.1016/j.neuron. 2017.02.034 [PubMed: 28334609]

45. Tsai H-C, et al. Phasic firing in dopaminergic neurons is sufficient for behavioral conditioning. Science (New York, N.Y.). 2009; 324:1080–1084. DOI: 10.1126/science.1168878

46. Han S, Soleiman MT, Soden ME, Zweifel LS, Palmiter RD. Elucidating an Affective Pain Circuit that Creates a Threat Memory. Cell. 2015; 162:363–374. DOI: 10.1016/j.cell.2015.05.057 [PubMed: 26186190]

47. Tritsch NX, Granger AJ, Sabatini BL. Mechanisms and functions of GABA co-release. Nature reviews. Neuroscience. 2016; 17:139–145. DOI: 10.1038/nrn.2015.21 [PubMed: 26865019]

48. Gozzi A, et al. A neural switch for active and passive fear. Neuron. 2010; 67:656–666. DOI: 10.1016/j.neuron.2010.07.008 [PubMed: 20797541]

49. Yu K, et al. The central amygdala controls learning in the lateral amygdala. Nature neuroscience. 2017; 20:1680–1685. DOI: 10.1038/s41593-017-0009-9 [PubMed: 29184202]

50. Asmundson GJ, Bonin MF, Frombach IK, Norton GR. Evidence of a disposition toward fearfulness and vulnerability to posttraumatic stress in dysfunctional pain patients. Behaviour research and therapy. 2000; 38:801–812. [PubMed: 10937428]

51. Bi LL, et al. Amygdala NRG1-ErbB4 is critical for the modulation of anxiety-like behaviors. Neuropsychopharmacology. 2015; 40:974–986. DOI: 10.1038/npp.2014.274 [PubMed: 25308353]

52. Grippo RM, Purohit AM, Zhang Q, Zweifel LS, Guler AD. Direct Midbrain Dopamine Input to the Suprachiasmatic Nucleus Accelerates Circadian Entrainment. Current biology : CB. 2017; 27:2465–2475 e2463. DOI: 10.1016/j.cub.2017.06.084 [PubMed: 28781050]

53. Fellmann C, et al. An optimized microRNA backbone for effective single-copy RNAi. Cell reports. 2013; 5:1704–1713. DOI: 10.1016/j.celrep.2013.11.020 [PubMed: 24332856]

54. Meis S, Endres T, Lessmann V. Postsynaptic BDNF signalling regulates long-term potentiation at thalamo-amygdala afferents. The Journal of physiology. 2012; 590:193–208. DOI: 10.1113/jphysiol.2011.220434 [PubMed: 22083603]

55. Dobin A, et al. STAR: ultrafast universal RNA-seq aligner. Bioinformatics. 2013; 29:15–21. DOI: 10.1093/bioinformatics/bts635 [PubMed: 23104886]

56. Kim D, et al. TopHat2: accurate alignment of transcriptomes in the presence of insertions, deletions and gene fusions. Genome biology. 2013; 14:R36.doi: 10.1186/gb-2013-14-4-r36 [PubMed: 23618408]

57. Anders S, Pyl PT, Huber W. HTSeq--a Python framework to work with high-throughput sequencing data. Bioinformatics. 2015; 31:166–169. DOI: 10.1093/bioinformatics/btu638 [PubMed: 25260700]

58. Tovote P, et al. Midbrain circuits for defensive behaviour. Nature. 2016; 534:206–212. DOI: 10.1038/nature17996 [PubMed: 27279213]

59. Cho JR, et al. Dorsal Raphe Dopamine Neurons Modulate Arousal and Promote Wakefulness by Salient Stimuli. Neuron. 2017; 94:1205–1219 e1208. DOI: 10.1016/j.neuron.2017.05.020 [PubMed: 28602690]

60. Behbehani MM. Functional characteristics of the midbrain periaqueductal gray. Prog Neurobiol. 1995; 46:575–605. [PubMed: 8545545]

61. Davis M. Neural systems involved in fear and anxiety measured with fear-potentiated startle. The American psychologist. 2006; 61:741–756. DOI: 10.1037/0003-066X.61.8.741 [PubMed: 17115806]

62. Davis M, Walker DL, Miles L, Grillon C. Phasic vs sustained fear in rats and humans: role of the extended amygdala in fear vs anxiety. Neuropsychopharmacology. 2010; 35:105–135. DOI: 10.1038/npp.2009.109 [PubMed: 19693004]
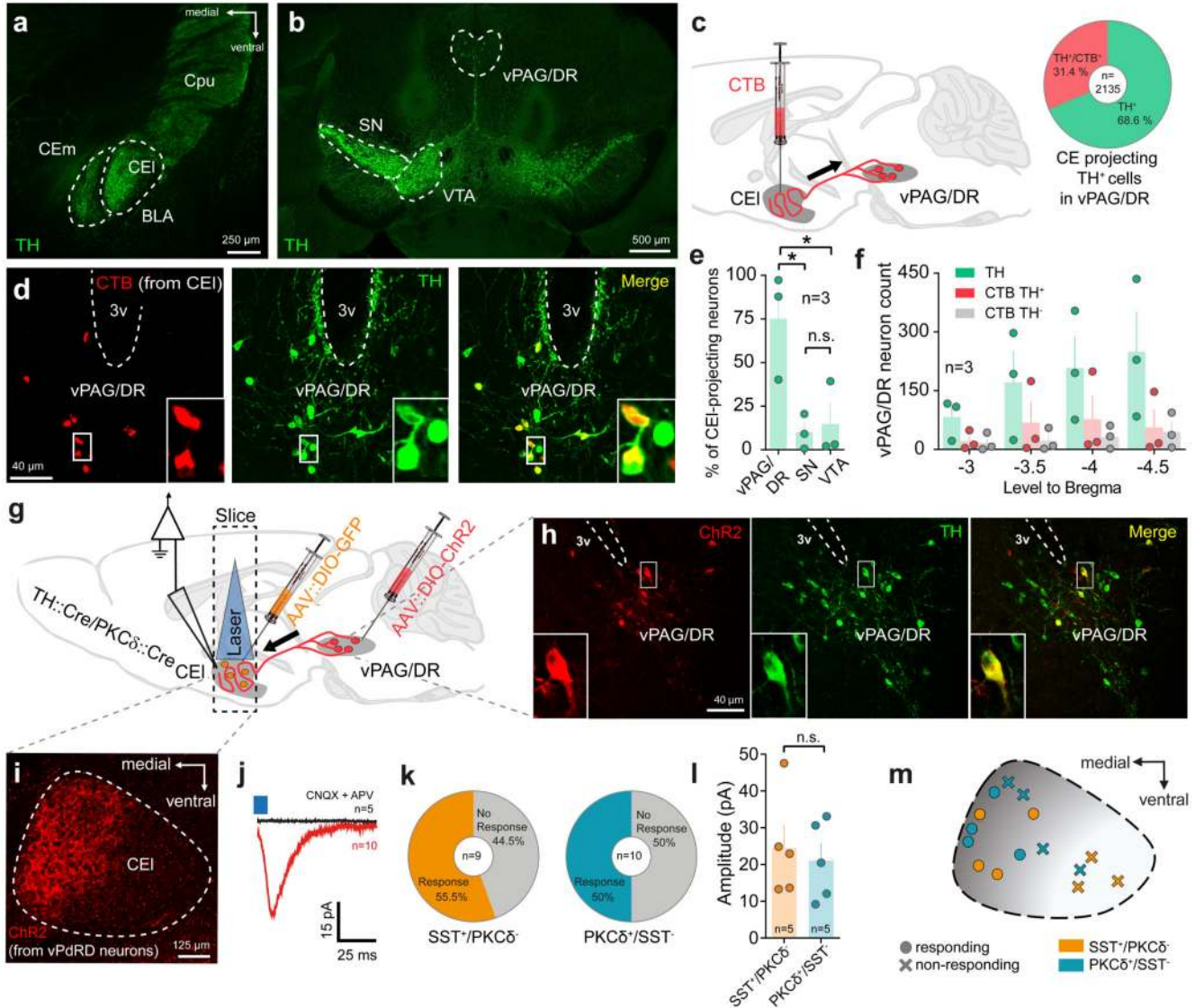
Figure 1. vPAG/DR-CE circuitry is a major DA-ergic component in the fear pathway.
Representative images of (**a**) CEl as a target of TH immunopositive terminals in the temporal lobe, of (**b**) TH immunopositive neurons in the midbrain and (**c**) of the identification of CEl DA sources by CTB retrograde tracing. Inset indicates fraction of CEl-projecting vPdRD neurons (**d**) CTB retrogradely labelled neurons in the vPAG/DR and co-localized with TH immunoreactivity. (**e**) Distribution of CEl projecting CTB[+]/TH^{+} neurons in the major midbrain DA regions (n = 3 animals; values from 3 sections/animal; one-way ANOVA F (2, 6) = 7.962, P = 0.0205; Holm-Sidak post-hoc test;) (**f**) Anterior to posterior distribution of TH[+]/CTB^{+} PAG neurons after CEl CTB injection. (**g**) Combined CTB/ChR2 optogenetic circuit mapping of vPdRD neurons in AAV::DIO-ChR2, AAV::DIO-GFP injected TH::Cre/PKCδ::Cre double transgenic animals. (h-i) ChR2^{+} fibers of infected vPdRD neurons (**h**) innervate the CEl (**i**) (cf. TH[+] terminals in (**a**)). (**j**) Post-synaptic currents recorded in whole cell patch-clamp configuration from CEl neurons (red, average

trace; n=10 neurons) induced by optogenetic activation of ChR2$^+$ fiber terminals of vPdRD neurons (**i**). PSC elicited in aCSF can be blocked by application of 10 μM CNQX + 50 μM APV (black, average trace; n=10 neurons). (**k**) Fraction of CEl SST$^+$/PKCδ$^-$ and PKCδ$^+$/SST$^-$ neurons responding to optogenetic activation in CEl. (**l**) Evoked ePSC amplitude of responding CEl SST$^+$/PKCδ$^-$ and PKCδ$^+$/SST$^-$ neurons (n=5 neurons; unpaired t-test, two-sided, t (8)= 0.4281, P=0.6799. (**m**) Spatial distribution of a subset of responding (**l**) and non-responding cells in CEl (cf. distribution of TH$^+$(**a**) and ChR2$^+$ (**i**) terminals). Representative images from at least three independent experiments (animals). Bars are means ± s.e.m. Significance levels between groups at * P<0.05.
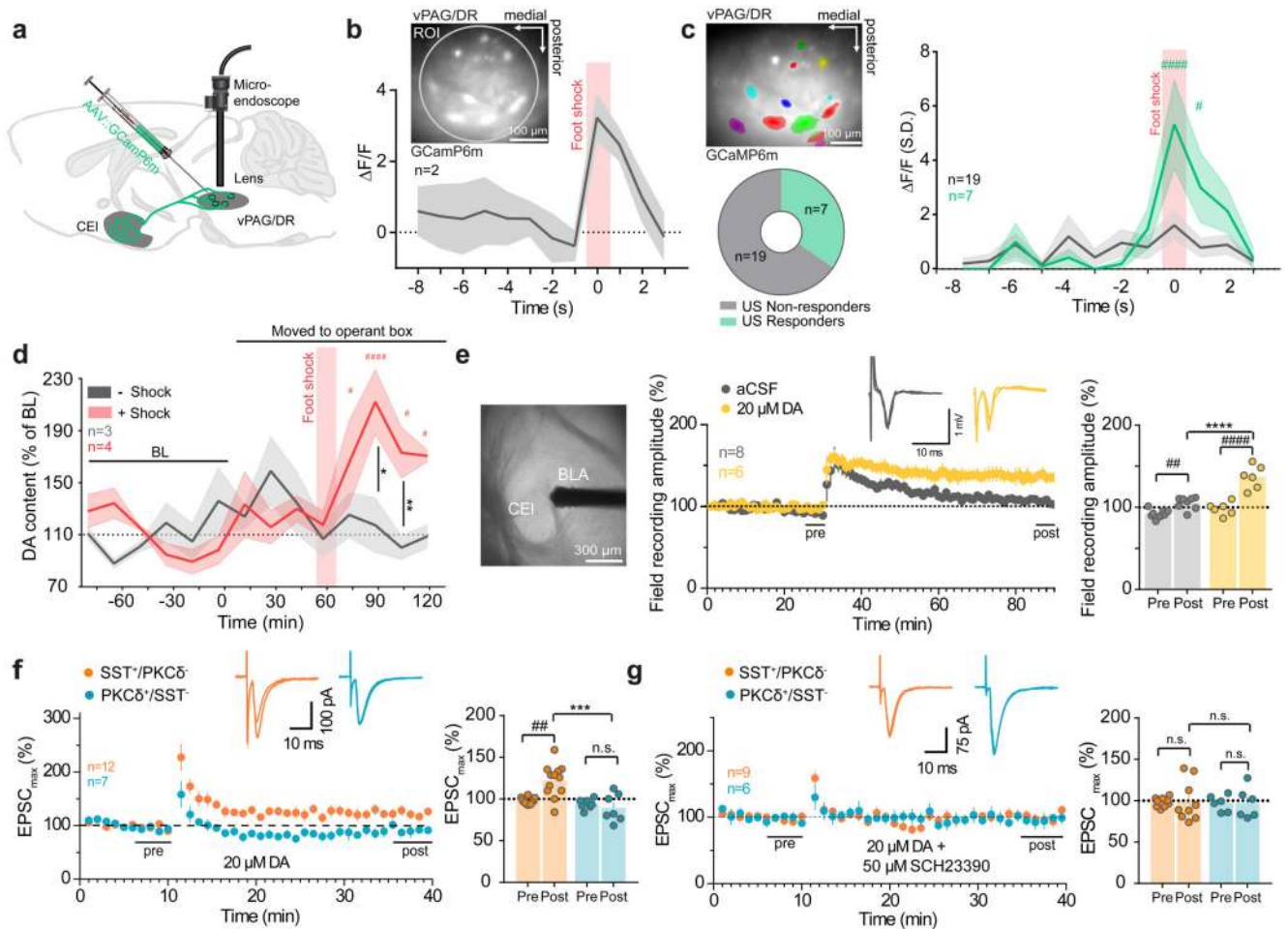
Figure 2. Modulation of vPAG/DR-CE circuitry by shock and DA.

(**a**) Deep brain Ca^{2+} imaging of vPAG/DR neurons. (**b**) Bulk Ca^{2+} imaging of vPAG/DR neuronal activity of freely moving mice in response to foot shock (n = 2 animals). Inset shows bulk imaging of vPAG/DR neurons expressing GCaMP6m. Circle indicates ROI used to calculate the bulk signal. (**c**) (*top left*) Representative example of vPAG/DR neuronal units expressing GCaMP6m (n= ROIs from 2 animals). Fraction of neuronal units responding (n = 7 cells) and non-responding (n = 19 cells) to foot shock (*bottom left*) and corresponding Ca^{2+} signals (*right*) (RM two-way ANOVA ($F_{interaction}$ (11, 264) = 3.141, P = 0.0005; F_{time} (11, 264) = 6.798, P < 0.0001; $F_{columns}$ (1, 24) = 3.235, P = 0.0847; Holm-Sidak post-hoc tests) (**d**) Microdialysis of DA release in the rat amygdala upon foot shock (n = 4 animals + shock session, n=3 animals -shock session; re-exposure; RM two-way ANOVA ($F_{interaction}$ (8, 40) = 4.26, P = 0.0009; F_{time} (8, 40) = 2.461, P = 0.0286; F_{groups} (1, 5) = 2.633, P = 0.1656; Holm-Sidak post-hoc tests). (**e**) CEl LFP recordings from acute slices with HFS (100 Hz, 1 s, 3 times, every 30 s) ± 20 μM DA (aCSF control group: n= 8 cells, DA group: n=6 cells; tests for LTP: RM two-way ANOVA $F_{interaction}$ (1, 12) = 20.2, P = 0.0007, F_{time} (1, 12) = 81.69, P < 0.0001; F_{groups} (1, 12) = 23.35, P = 0.0004; Holm-Sidak post-hoc tests). (**f-g**) LTP recordings of CEl neurons in the presence of (**f**) 20 μM DA ($SST^+/PKC\delta^-$ cells: n = 12, $SST^-/PKC\delta^+$ cells: n = 7; tests for LTP: RM two-way ANOVA $F_{interaction}$ (1, 14) =

9.052, $P = 0.0094$, F_{time} (1, 14) = 3.807, $P = 0.0713$; F_{groups} (1, 14) = 11.6, $P = 0.0043$; Holm-Sidak post-hoc tests) and (**g**) 20 µM DA + 50 µM SCH 23390 DA (SST$^+$/PKCδ$^-$ cells: n = 9, SST$^-$/PKCδ$^+$ cells: n = 6; tests for LTP: RM two-way ANOVA $F_{interaction}$ (1, 11) = 0.0001787 $P = 0.9896$, F_{time} (1, 11) = 0.0008886, $P = 0.9768$; F_{groups} (1, 11) = 0.01172, $P = 0.9158$; Holm-Sidak post-hoc tests). (**c-g**). Lines with shaded regions represent means ± upper and lower bounds (**b**) or s.e.m (**c-d**). Bars are means ± s.e.m. Significance levels between groups (*) and to baseline (BL) or pre-HFS (#) at */# $P<0.05$, **/## $P<0.01$, ***/### $P<0.001$ and ****/#### $P<0.0001$.
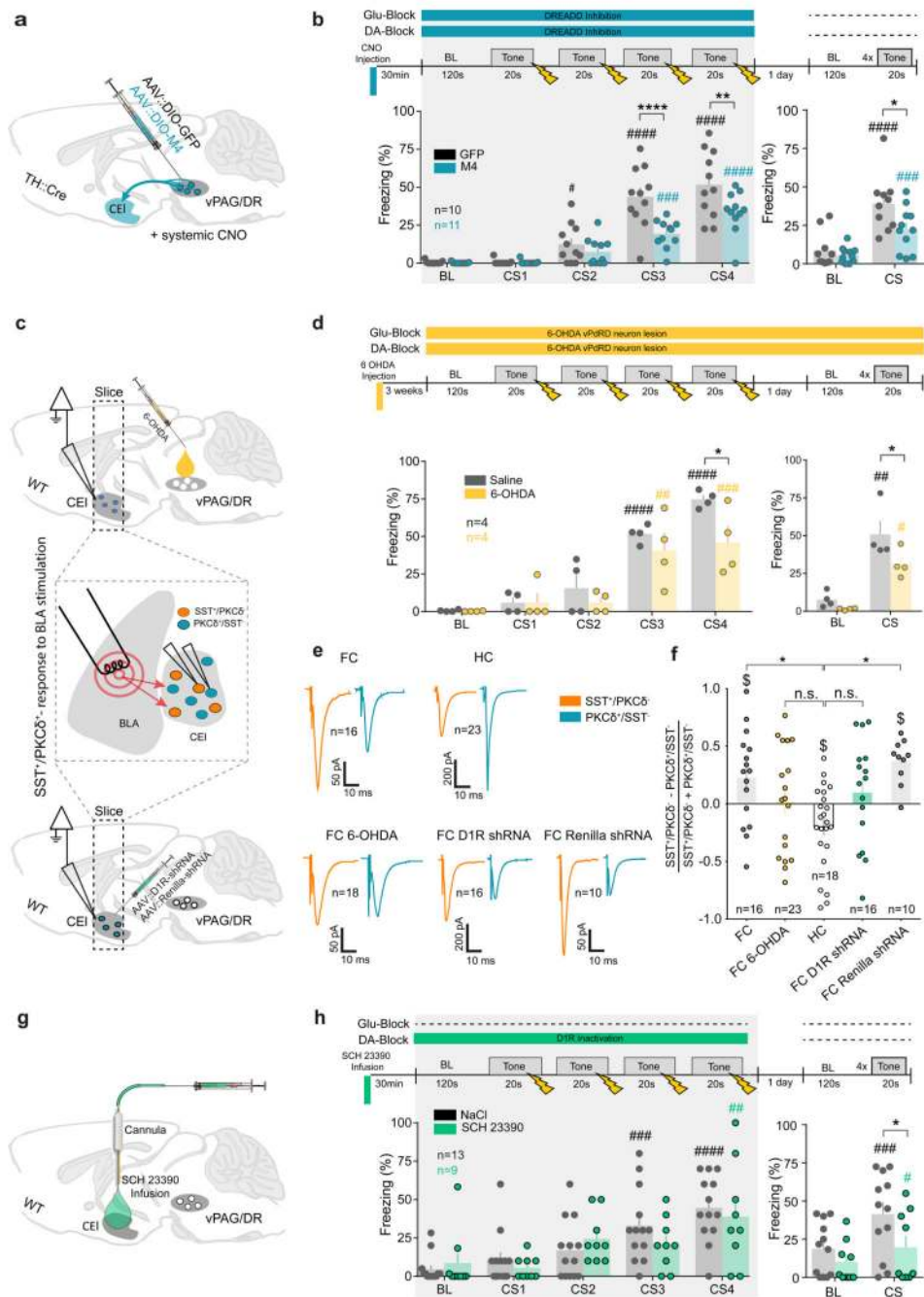
Figure 3. vPdRD neurons support fear memory formation and amygdala rewiring.
(**a**) AVV mediated Cre-dependent expression of DREADD M4 in vPdRD neurons of
TH::Cre transgenic animals. (**b**) Fear conditioning protocol and freezing responses for
systemic CNO injection and subsequent M4-receptor dependent tonic vPdRD neuron
inhibition during conditioning (control group: n = 10 animals, M4 group: n = 11 animals;
RM two-way $ANOVA_{conditioning}$ $F_{interaction}$ (4, 80) = 6.276, P = 0.002; F_{time} (4, 80) = 75.96,
P = 0.0001; F_{groups} (1, 20) = 9.119, P = 0.0068; RM two-way $ANOVA_{recall}$ $F_{interaction}$ (1, 19)
= 7.161, P = 0.0149; F_{time} (1, 19) = 83.32, P < 0.0001; F_{groups} (1, 19) = 3.717, P = 0.0689;

Holm-Sidak post-hoc tests). (**c**) Experience dependent plasticity of BLA-CEl SST$^+$ synapses upon fear conditioning after either 6-OHDA ablation of vPdRD neurons (*top*) or AAV mediated D1R knock down in the CEl (*bottom*). (d) Freezing responses after 6-OHDA lesioning of vPdRD neurons during conditioning (control group: n = 4 animals, 6-OHDA lesion group: n = 4 animals; RM two-way ANOVA$_{conditioning}$ F$_{interaction}$ (4, 24) = 1.619, $P =$ 0.2021; F$_{time}$ (4, 24) = 34.05, $P < 0.0001$; F$_{groups}$ (1, 6) = 6.029, $P = 0.0494$; Holm-Sidak post-hoc tests) and testing (RM two-way ANOVA$_{recall}$ F$_{interaction}$(1, 6) = 1.344, $P = 0.2904$, F$_{time}$ (1, 6) = 40.88, $P=0.0007$; F$_{groups}$(1, 6) = 7.098, $P = 0.0373$; Holm-Sidak post-hoc tests). (**e**) Averaged whole-cell patch-clamp recordings of post-synaptic currents of CEl SST$^+$/PKCδ$^-$ and PKCδ$^+$/SST$^-$ neurons next to each other (<60μm) in response to BLA stimulation of animals that underwent fear conditioning (FC, n = 16 cell pairs), that were naïve (home cage, HC, n = 23 cell pairs), that received 6-OHDA ablation of vPdRD neurons and underwent fear conditioning (FC 6-OHDA, n = 18 cell pairs), that received D1R knockdown virus in the CEl and underwent fear conditioning (FC D1R shRNA, n = 16 cell pairs) and that received a control virus and underwent fear conditioning (FC renilla shRNA, n = 10 cell pairs). (**f**) Ratio of CEl SST$^+$/PKCδ$^-$ to PKCδ$^+$/SST$^-$ neuron post-synaptic currents after mice underwent a given behavioral paradigm as described in (**e**) (n = cell pair groups described in (**e**); One-way ANOVA$_{pairs}$ F$_{groups}$ (4, 78) = 4.624 $P = 0.0021$; Dunnett's post-hoc). (**g**) Targeted pharmacological inhibition of CEl D1Rs by local infusion of SCH23390. (**h**) Freezing responses after CEl targeted SCH23390 infusion during conditioning (RM two-way ANOVA $_{conditioning}$ F$_{interaction}$ (4, 80) = 1.106, $P=0.3593$; F$_{time}$ (4, 80) = 14.79, $P < 0.0001$; F$_{groups}$ (1, 20) = 0.1926, $P = 0.6655$; Holm-Sidak post-hoc tests) and drug-free testing sessions (RM two-way ANOVA$_{recall}$ F$_{interaction}$(1, 19) = 6.164, $P = 0.0225$, F$_{time}$ (1, 19) = 36.94, $P<0.0001$; F$_{groups}$ (1, 19) = 2.88, $P = 0.1060$; Holm-Sidak post-hoc tests). Bars are means ± s.e.m. Significance levels between groups (*) and to baseline (BL) (#) at */# $P<0.05$, **/## $P<0.01$, ***/### $P<0.001$ and ****/#### $P<0.0001$.
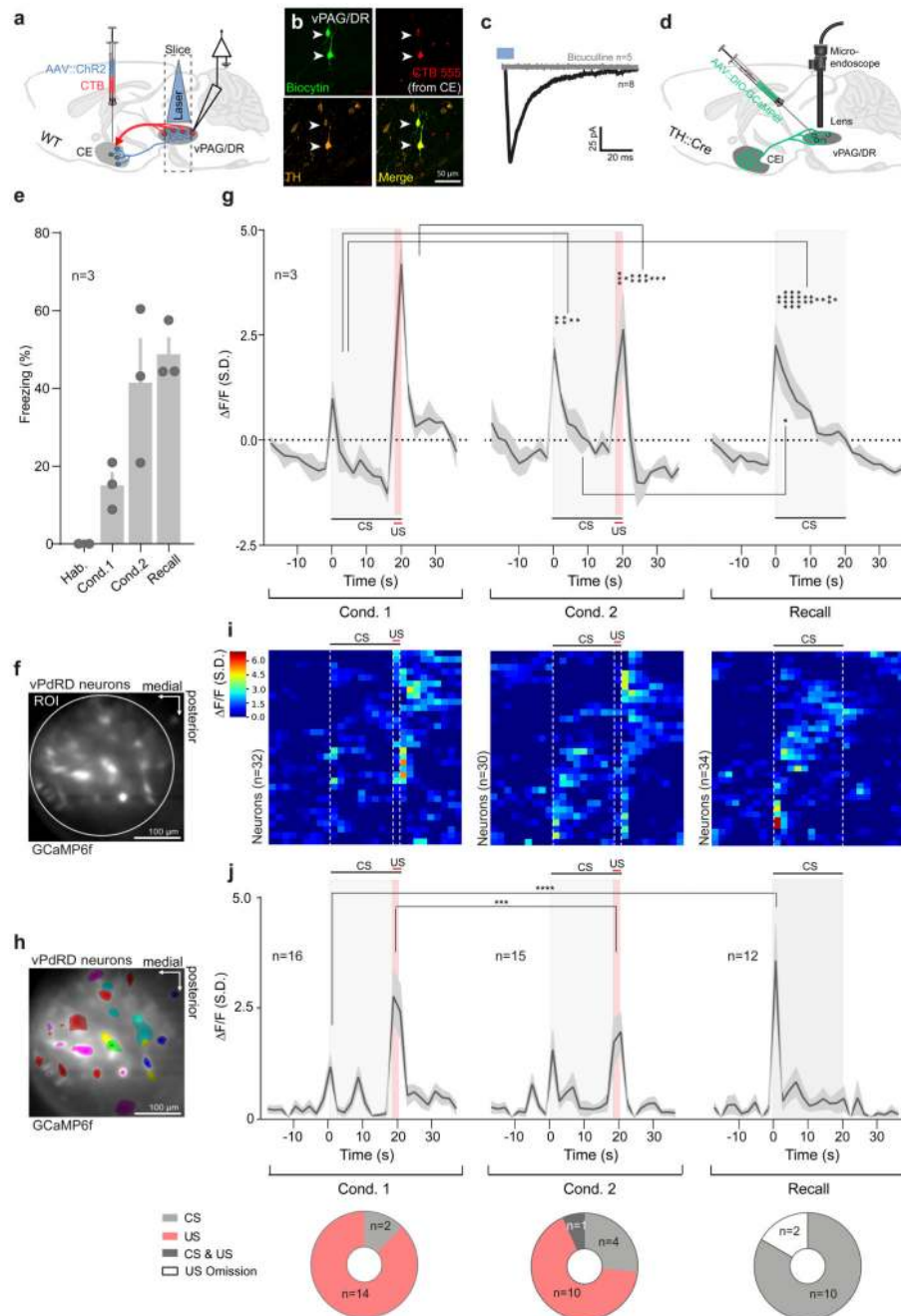
Figure 4. vPdRD neurons encode PE linked teaching signals.
(**a**) Combined CE CTB/ChR2 injections and whole cell patch-clamp recordings in the vPAG/DR. (**b**) Representative image of Biocytin-filled, TH[+] and CTB retrogradely labelled (derived from CE targeted CTB injections) vPdRD neurons. (**c**) Optogenetic activation of CE originating ChR2 fibers elicits iPSCs in vPdRD neurons (red, average trace, n = 8 cells) blocked by application of 50 μM Bicuculline (black, average trace, n = 5 cells). (**d**) Expression of GCaMP6 in vPdRD neurons in TH::Cre animals injected with dependent AAV. (**e**) Freezing levels of Ca^{2+} imaged animals during fear conditioning and recall. (**f**)

Bulk imaging of vPdRD neurons expressing GCaMP6f. Circle indicates ROI used to calculate the bulk signal. (**g**) Trial averages of bulk Ca^{2+} signals of vPAG/DR neuronal activity during fear conditioning and recall (n = ROIs from 3 animals; RM two-way ANOVA $F_{interaction}$ (54, 56) = 3.204, P<0.0001; F_{rows} (27, 28) = 3.434, F_{time} (2, 56) = 1.974, P=0.1484; Holm-Sidak post-hoc tests). (**h**) Representative example of vPdRD neuronal units expressing GCaMP6f. (**i**) Clustered traces of Ca^{2+} signals from vPdRD neuronal units from experiment shown in (**g**). (**j**) (*top*) Trail averages of Ca^{2+} event amplitudes of a CS and/or US responsive subset of vPdRD neurons (n = units from 3 animals; RM two-way ANOVA $F_{interaction}$ (54, 1080) = 3.749, P<0.0001; F_{time} (27, 1080) = 15.43, P<0.0001; F_{column} (2, 40) = 1.15, P = 0.3270; Holm-Sidak post-hoc tests). (*bottom*) Fraction of subsets of single units responding to either CS and/or US (n = units from 3 animals; Chi-Square (20.05, 4), P=0.005). Representative images from three independent experiments (animals). Bars and lines with shaded regions represent means ± s.e.m Significance levels between groups (*) at * P<0.05, ** P<0.01, *** P<0.001 and **** P<0.0001. Ca^{2+} signals and event amplitudes are derived from per ROI (**g**) or per cell (**i-j**) dF/F values, standardized over the whole experiment and given as units S.D.
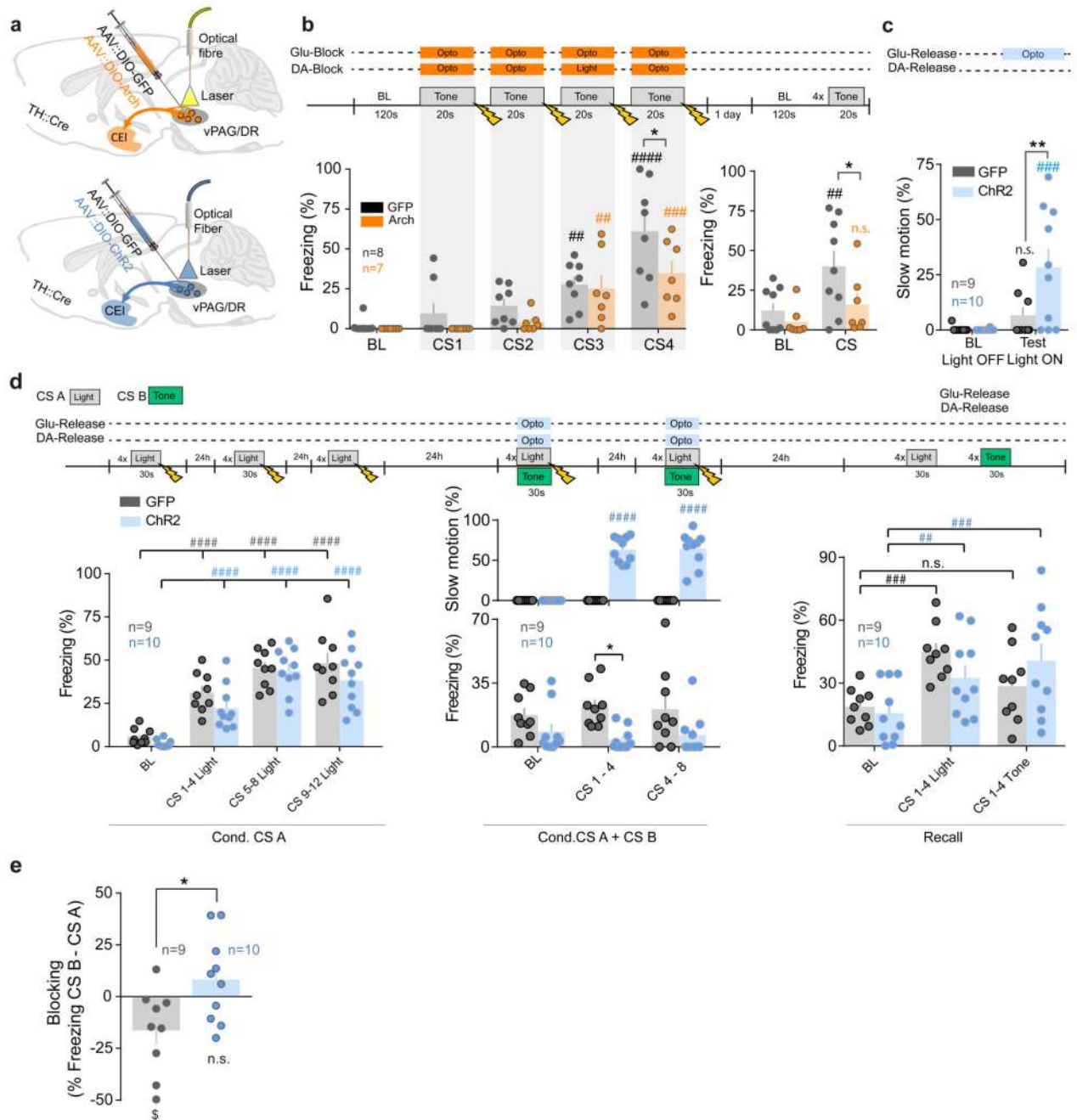
Figure 5. vPdRD neuron reinforcement signals direct associative learning.
Optogenetic targeting of vPdRD neurons in TH::Cre animals injected with AAV for Cre-dependent expression of (**a**) eArch3.0 or ChR2 (**b**) Freezing responses to neuronal inhibition by eArch3.0 during CS-US presentations (control group: n = 8 animals, Arch group: n = 7 animals; RM two-way ANOVA$_{conditioning}$ F$_{interaction}$ (4, 52) = 1.612, P = 0.1853; F$_{time}$ (4, 52) = 24.97, P < 0.0001; F$_{groups}$ (1, 13) = 4.189, P = 0.0615; two-way ANOVA$_{recall}$ F$_{interaction}$ (1, 14) = 2.846, P = 0.1137; F$_{time}$ (1, 14) = 14.57, P = 0.0019; F$_{groups}$ (1, 14) = 3.18, P = 0.0962; Holm-Sidak post-hoc tests). (**c**) Quantification of a slow motion behavioral

state (cf. Fig. 5d) upon vPdRD neuron activation (control group: n = 9 animals, Chr2 group: n = 10 animals; RM two-way ANOVA $F_{interaction}$ (1, 17) = 5.309, $P = 0.0341$; F_{time} (1, 17) = 13.01, $P=0.0022$; F_{groups} (1, 17) = 4.969, $P = 0.0396$; Holm-Sidak post-hoc tests). (d) Design of associative blocking experiment (control group: n = 9 animals, Chr2 group: n = 10 animals). Acquisition of fear to CS A during first training session (RM two-way ANOVA $F_{interaction}$ (3, 51) = 0.6537, $P = 0.5843$, F_{time} (3, 51) = 57.27, $P < 0.0001$; F_{groups} (1, 17) = 2.927, $P = 0.1053$; Holm-Sidak post-hoc tests). Fear response and slow motion postures during compound conditioning phase (fear response: RM two-way ANOVA $F_{interaction}$ (2, 34) = 1.198, $P = 0.3142$; F_{time} (2, 34) = 0.03155, $P = 0.9690$; F_{groups} (1, 17) = 7.392, $P = 0.0146$; Holm-Sidak post-hoc tests; slow motion: RM two-way ANOVA $F_{interaction}$ (2, 34) = 54.57, $P < 0.0001$; F_{time} (2, 34) = 54.57, $P < 0.0001$; F_{groups} (1, 17) = 193.7, $P < 0.0001$; Holm-Sidak post-hoc tests) with presentation of CS A and CS B. Fear response during testing phase to alternating presentation of CS A and CS B (RM two-way ANOVA $F_{interaction}$ (2, 34) = 4.624, $P = 0.0167$; F_{time} (2, 34) = 15.68, $P < 0.0001$; F_{groups} (1, 17) = 0.02811, $P = 0.8688$; Holm-Sidak post-hoc tests). (**e**) Quantification of blocking effect from recall in c (unpaired t-test, two-sided t(17)= 2.58, $P_{Control\ vs\ ChR2}$ =0.0195; one-sample t-tests against zero t (8) = 2.407 $P_{Control}$ = 0.0427 ($) , t(9) = 1.235 P_{ChR2} = 0.2482). Bars are means ± s.e.m. Significance levels between groups (*) and to baseline (BL) or between trials or sessions (#) at */# $P<0.05$, **/## $P<0.01$, ***/### $P<0.001$ and ****/#### $P<0.0001$.